Mechanism of the reaction, $CH_4+O(^1D_2)\rightarrow CH_3+OH$, studied by ultrafast and state-resolved photolysis/probe spectroscopy of the $CH_4\cdot O_3$ van der Waals complex

C. Cameron Miller, Roger D. van Zee, and John C. Stephenson[a)]
National Institute of Standards and Technology, Gaithersburg, Maryland 20899

The mechanism of the reaction $CH_4+O(^1D_2)\rightarrow CH_3+OH$ was investigated by ultrafast, time-resolved and state-resolved experiments. In the ultrafast experiments, short ultraviolet pulses photolyzed ozone in the $CH_4\cdot O_3$ van der Waals complex to produce $O(^1D_2)$. The ensuing reaction with CH_4 was monitored by measuring the appearance rate of $OH(v=0,1;J,\Omega,\Lambda)$ by laser-induced fluorescence, through the $OH\,A\leftarrow X$ transition, using short probe pulses. These spectrally broad pulses, centered between 307 and 316 nm, probe many different OH rovibrational states simultaneously. At each probe wavelength, both a fast and a slow rise time were evident in the fluorescence signal, and the ratio of the fast-to-slow signal varied with probe wavelength. The distribution of $OH(v,J,\Omega,\Lambda)$ states, $P_{obs}(v,J,\Omega,\Lambda)$, was determined by laser-induced fluorescence using a high-resolution, tunable dye laser. The $P_{obs}(v,J,\Omega,\Lambda)$ data and the time-resolved data were analyzed under the assumption that different formation times represent different reaction mechanisms and that each mechanism produces a characteristic rovibrational distribution. The state-resolved and the time-resolved data can be fit independently using a two-mechanism model: $P_{obs}(v,J,\Omega,\Lambda)$ can be decomposed into two components, and the appearance of OH can be fit by two exponential rise times. However, these independent analyses are not mutually consistent. The time-resolved and state-resolved data can be consistently fit using a three-mechanism model. The OH appearance signals, at all probe wavelengths, were fit with times $\tau_{fast}\approx 0.2$ ps, $\tau_{inter}\approx 0.5$ ps and $\tau_{slow}\approx 5.4$ ps. The slowest of these three is the rate for dissociation of a vibrationally excited methanol intermediate (CH_3OH^*) predicted by statistical theory after complete intramolecular energy redistribution following insertion of $O(^1D_2)$ into CH_4. The $P_{obs}(v,J,\Omega,\Lambda)$ was decomposed into three components, each with a linear surprisal, under the assumption that the mechanism producing OH at a statistical rate would be characterized by a statistical prior. Dissociation of a CH_4O^* intermediate before complete energy randomization was identified as producing OH at the intermediate rate and was associated with a population distribution with more rovibrational energy than the slow mechanism. The third mechanism produces OH promptly with a cold rovibrational distribution, indicative of a collinear abstraction mechanism. After these identifications were made, it was possible to predict the fraction of signal associated with each mechanism at different probe wavelengths in the ultrafast experiment, and the predictions proved consistent with measured appearance signals. This model also reconciles data from a variety of previous experiments. While this model is the simplest that is consistent with the data, it is not definitive for several reasons. First, the appearance signals measured in these experiments probe simultaneously many $OH(v,J,\Omega,\Lambda)$ states, which would tend to obfuscate differences in the appearance rate of specific rovibrational states. Second, only about half of the $OH(v,J,\Omega,\Lambda)$ states populated by this reaction could be probed by laser-induced fluorescence through the $OH\,A\leftarrow X$ band with our apparatus. Third, the cluster environment might influence the dynamics compared to the free bimolecular reaction. [DOI: 10.1063/1.1331615]

I. INTRODUCTION

The reaction between hydrocarbons and $O(^1D_2)$ is central to the chemistry of the upper atmosphere. As such, the mechanism and dynamics of the major reaction channel[1] of the simplest hydrocarbon, $CH_4(\tilde{X}\,^1A_1)+O(^1D_2)\rightarrow CH_3(\tilde{X}\,^2A_2'')+OH(X^2\Pi)$, have been extensively studied. The reaction is exothermic[2] ($\Delta H^o_{0\,K}=-182$ kJ mol^{-1} $=-15\,240$ cm^{-1}) with a rate constant close to a gas kinetic value and independent of temperature. Certain limiting, archetypical mechanisms can be envisioned for the reaction of O atoms with CH_4, including insertion/elimination, abstraction, and stripping. In the insertion/elimination archetype, the oxygen atom inserts into a C–H bond to form a vibrationally excited methanol intermediate (CH_3OH^*) that undergoes complete intramolecular vibrational energy redistribution (IVR) before dissociating. Both the distribution of energy in the fragments and the CH_3OH^* unimolecular dissociation

---

[a)]Electronic mail: john.stephenson@nist.gov

rate would be expected to follow the predictions of statistical theory. For the abstraction mechanism, the oxygen atom would travel towards the methane molecule along the carbon–hydrogen bond to extract a hydrogen atom and then recoil to form the hydroxyl radical. The reaction should be virtually instantaneous, and the distribution of rovibrational energy in the fragments would be colder than the statistical expectation. In the case of a stripping mechanism, the oxygen atom would fly by the methane molecule, snatching a hydrogen atom on the way. As with abstraction, a stripping reaction should be fast, but unlike an abstraction, should result in substantial rovibrational excitation in the hydroxyl product.

Nature is not confined to a single limiting case and early work supported parallel mechanisms. Initial evidence for a CH_3OH^* intermediate came from chemical quenching and matrix experiments[3–5] of the CH_4 and $O(^1D_2)$ reaction, which found that as the pressure in the reaction chamber increased, the quantum yield of CH_3OH increased. This observation was attributed to collisional stabilization of a CH_3OH^* intermediate. However, even in liquid argon some OH was formed, suggesting that at least a fraction of the product formed through an abstraction mechanism. Park and Wiesenfeld[6] studied the OH rovibrational product states from several hydrocarbons and concluded that, in the case of methane, most of the OH was characterized by a nonstatistical distribution. They postulated, however, that all the OH passed through a methanol intermediate, with most dissociation occurring prior to complete IVR. This conclusion was consistent with Luntz's earlier conjecture that most OH was formed by the latter mechanism, although OH in low-rotational levels was formed by an abstraction mechanism.[7] Sub-Doppler spectroscopy[8–12] has shown that $OH(v=0)$ was scattered nearly isotropically in the center-of-mass frame, but with some backward asymmetry, again suggesting both a long-lived intermediate and a reactive complex with a lifetime less than one rotational period. By comparison to OH, little is known about the CH_3 product. Absorption spectra recorded with an infrared diode laser[13] have been used to determine the nascent distribution of the out-of-plane bend (v_2). It was found that $v=0$ was the most populated level of that mode, with monotonically decreasing population up to $v=4$. This measured distribution was significantly colder than an unconstrained, statistical prior distribution. Multiphoton ionization spectra[14,15] of the out-of-plane bend and symmetric stretch also suggested that there was comparatively little vibration excitation in the CH_3 fragment, though because the Franck–Condon factors and autodissociation rates of the excited state were unknown, no quantitative conclusions could be reached. An *ab initio* calculation[16] of the potential-energy surface for the CH_4+O reaction suggested that insertion-, abstraction-, and stripping-like mechanisms were possible. Recent quasiclassical trajectory calculations found that insertion is the dominant mechanism,[17,18] though there were distinct classes of trajectories, one being direct and producing an inverted rovibrational distribution and the other being indirect and producing a noninverted distribution. Although inconclusive, these investigations suggest complicated reaction dynamics.
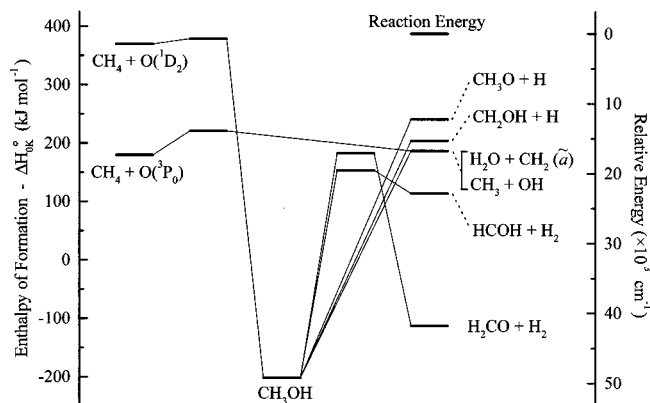
FIG. 1. A correlation diagram for the reaction between methane and atomic oxygen. The heats of formation and barrier heights are based on Refs. 2, 89, 92–96.

Although OH and CH_3 are the major products (estimates vary from 69%–96%), several minor products have also been identified. Figure 1 shows a correlation diagram indicating the energetics for various channels. Primary H atom production has been studied by laser-induced fluorescence experiments.[19–21] Whether the co-fragment was CH_3O or CH_2OH was controversial until recent crossed molecular beam experiments[22,23] found CH_2OH+H to be the second most probable channel. Most of the H atom product is isotropically scattered, though about a tenth is back scattered. This finding supports parallel mechanisms for this channel too. The beam experiments also found that H_2CO+H_2 are primary products. All the H_2 was found to be isotropically distributed, and this channel was concluded to evolve through a CH_3OH^* intermediate after complete IVR. The methoxy radical has also been reported to be a direct product of this reaction, although this is uncertain. Because the O–H bond is not the weakest bond in the molecule, this would imply dissociation of an intermediate in which energy has not fully randomized. In addition, the reaction to form $CH_2(\tilde{a})+H_2O$ as minor primary products has been reported.[23–25] The observation of these minor products implies that dissociation of a methanol intermediate after energy randomization is an important mechanism for reactive collisions between CH_4 and $O(^1D_2)$.

We previously reported preliminary findings from experiments aimed at further elucidating the mechanism of the primary reaction channel. An ultrafast laser system was used to measure OH production as a function of time following ultrafast photolysis at 267 nm of the $CH_4\cdot O_3$ van der Waals complex.[26] Prompt dissociation of ozone produces $O(^1D_2)$, which then reacts with the neighboring CH_4 to form OH. This reaction was monitored by measuring OH laser-induced fluorescence, through the OH $A(^2\Sigma)\leftarrow X(^2\Pi)$ transition, as a function of photolysis/probe delay. Initiating the reaction in a cluster provides a clear time-zero against which to measure the appearance of the reaction products.[27–29] A single exponential rise with a time constant of several picoseconds adequately fit the $OH(v=0,J)$ states probed in those experiments. This appearance rate was consistent with the rate of dissociation of CH_3OH^* predicted by statistical rate theory. Given the time resolution and signal-to-noise of that experi-

ment, we concluded that any prompt OH channel produced less than 20% of that probed. We have also previously reported the rovibrational state distributions in the cluster reaction and found them quite similar to those of the free, bimolecular reaction,[30] an observation which Wada and Obi[31] subsequently confirmed and which suggests that the cluster environment replicates the dynamics of the free bimolecular reaction.

The present article expands on our preliminary studies,[26,30] and reports important new findings. Improved time resolution, increased signal-to-noise, and the ability to probe more OH($v=0$) rotational states and OH($v=1$) made these new time-resolved results possible. The appearance of OH was measured at six probe wavelengths spanning the OH($v=0,1$) manifolds. The new data clearly show, in addition to the previously reported statistical channel, OH formed by much faster mechanisms. We have also measured the OH($v=0,1$) rotational state distribution again.

II. EXPERIMENTAL APPARATUS AND PROCEDURES

A. Ultrafast experiments

The light source for the ultrafast photolysis/probe experiment consisted of a passively mode-locked, titanium doped sapphire (Ti:Al$_2$O$_3$) laser oscillator that produced transform-limited, 70 fs pulses centered at 800 nm. The pulses were stretched to >200 ps, amplified to 2 mJ at a repetition rate of 20 Hz in a Ti:Al$_2$O$_3$ regenerative amplifier, further amplified to 20 mJ in a Ti:Al$_2$O$_3$ rod using a three pass configuration, and then compressed to 100 fs. The amplifier rods were pumped by 10 ns, 532 nm pulses from a Nd^{3+}:YAG laser. The 267 nm photolysis light was generated by first doubling this compressed 800 nm light and then summing the resulting 400 nm light with residual 800 nm light. The probe was generated by focusing part of the 800 nm light into a cell containing deuterated water to create a white light continuum, which was passed through an interference filter to select light near 500 nm. This seed pulse was amplified in three, 1 cm long dye cuvettes, which were pumped by 355 nm pulses from a second Nd^{3+}:YAG laser. This light was then summed with 800 nm light in a 0.5 mm KH$_2$PO$_4$(KDP) crystal to give wavelengths between 307 and 316 nm ($\Delta\lambda_{FWHM} \approx 1.6$ nm) [full width at half maximum (FWHM)]. The interference filter was tilted to tune the center frequency of the transmitted light. Typically, fluences were 1 mJ cm^{-2} for the photolysis laser and 0.75 mJ cm^{-2} for the probe laser in these experiments. The orthogonally polarized pump and probe beams were combined on a dichroic mirror and propagated collinearly through the beam chamber.

The supersonic expansion in which the van der Waals complexes were formed was the same as in previous experiments.[26,30] The clusters formed in a supersonic expansion from reactants diluted in a 9:1 mixture of Ne:He. A 6% mix of O$_3$ in Ne:He flowed through one calibrated flow controller, pure CH$_4$ through another, and additional Ne:He through a third. The gases mixed just upstream of the pulsed valve, yielding a typical mix of 81% Ne, 9% He, 8% CH$_4$, and 2% O$_3$. Prior to use, gaseous O$_3$ was purified by distillation from liquid O$_3$. The total stagnation pressure was

≈ 310 kPa, and the chamber pressure was ≈ 1 mPa when the nozzle was pulsing. Under these mixture conditions, the OH signal was linear in the methane and ozone mole fraction. Additional evidence that the OH is formed in CH$_4 \cdot$O$_3$ clusters rather than larger clusters has been presented previously.[26,29] No signal was observed when either the methane or the ozone was removed from the expansion. The lasers, focused to a ≈ 1.5 mm diameter spot, intersected the molecular beam 8 mm downstream from the throat of the expansion.

The detection system was a photomultiplier tube perpendicular to the laser beams with two condensing doublet lenses to collect and image the fluorescence. Colored glass filters blocked stray photolysis light and wavelengths longer than ≈ 400 nm. On every laser pulse, gated boxcar integrators collected four channels of data: Laser-induced fluorescence (LIF) signal, the energy of the photolysis laser, the energy of the probe laser, and signal from the photolysis/probe cross-correlation.

Under the experimental conditions described above, the LIF signal was linear in the photolysis and probe energy, which indicates that neither the ozone nor the hydroxyl radical transitions were saturated. It also indicates that multiphoton processes are not a major contributor to the observed signals. While it is conceivable that a multiphoton process could lead to C–H bond rupture followed by reaction with ozone to produce hydroxyl, at the intensities we used such a process is insignificant compared to photolysis of ozone. It is conceivable that a multiphoton process could promote ozone to a higher electronic state, which would dissociate, presumably producing a different and probably very energetic oxygen atom. However, such a process would seem unlikely because of the rapidity of ozone dissociation. Moreover, one would expect that the product-state distribution from these alternative reactions would be quite different from that of the CH$_4$+O($^1D_2$) reaction. In previous experiments,[26] we determined the OH(v,J,Ω,Λ) distribution following photolysis with the ultrafast, 267 nm light and found this product-state distribution to be indistinguishable from that measured following photolysis by 7 ns pulses of the same fluence.[30] These observations suggest that the signal measured in the appearance curves reported here arises from reaction of CH$_4$+O($^1D_2$) following single-photon dissociation of O$_3$. At much higher photolysis intensities than those used here, the signals become nonlinear, and multiphoton processes occur, as evidenced by fluorescence occurring in the absence of the probe pulse.

Proper analysis of the rise curves demands an accurate measurement of the time of photoinitiation of the reaction. This time was determined by measuring the photolysis/probe cross-correlation by difference frequency mixing in a 0.1 mm KDP crystal, generating ≈ 1.9 μm light. To make this measurement, the Fresnel reflections from the front surface of the lithium fluoride window at the chamber entrance passed through a second lithium fluoride window identical to the chamber window. The difference frequency light was then generated in the KDP crystal, which was located at a point conjugate to the probe region in the chamber. The Gaussian full-width at half-maximum of the cross correlation
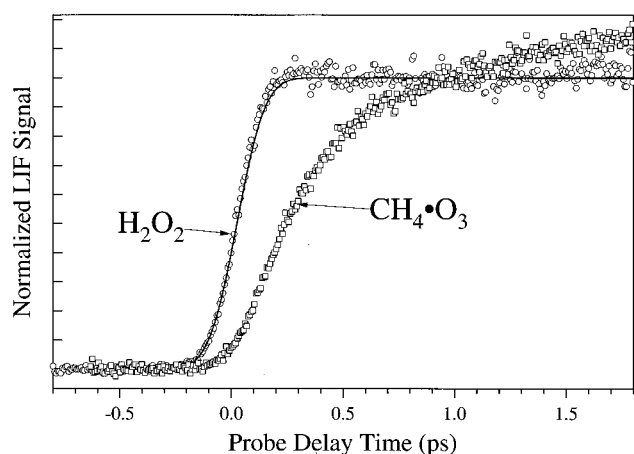
FIG. 2. The circles are the OH LIF signal from the photolysis of H_2O_2. The superimposed line is the photolysis/probe integrated cross correlation shifted by 25 fs. The squares are the OH LIF signal for the $CH_4 \cdot O_3$ cluster probed at 316.5 nm, the probe wavelength with the fastest appearance curve. The data are normalized so that the fast component in the cluster photolysis and the H_2O_2 signal have the same height at long time.

was routinely ≈ 200 fs. Accounting for the dispersion of air (1.0 fs cm^{-1}) and the dispersion of the KDP crystal (8 fs), time-zero could be determined to within 5 fs. To test this clocking apparatus, two additional experiments were carried out. First, a second 0.1 mm KDP crystal was placed in the vented chamber at the region of interaction, and the two cross-correlations were compared. The cross-correlations were aligned in time to ≈ 5 fs. Second, the LIF of OH formed by 267 nm photodissociation of hydrogen peroxide was measured. The ultraviolet photodissociation $H_2O_2 \rightarrow 2OH$ is known to be prompt.[32–35] To make these measurements, vapor from a mixture of 70% H_2O_2 in water flowed through the chamber at a pressure of ≈ 13 Pa. The rise curve of OH($v=0$) LIF from this reaction was indistinguishable from the integral of the laser cross-correlation, except for a shift in time attributable to the separation time of the OH fragments. The observed shift in time for the data set with probe laser centered at 308.9 nm is 25 fs± 15 fs. Using a standard approach,[36] we calculated a shift to be 30 fs. Therefore, the time-zero from the H_2O_2 experiments was consistent with the value measured using the crystal. The rise time of OH from the prompt dissociation of H_2O_2 is compared to the fastest observed formation time of OH from the $CH_4 \cdot O_3$ cluster experiment in Fig. 2. This figure illustrates that the time resolution was sufficient to determine even the fastest OH formation rates from the cluster. To the best of our knowledge, this represents the fastest temporal resolution with which the dissociation of H_2O_2 has been measured.[32]

B. State-resolved experiments

For the state-resolved photolysis/probe experiments, the fourth harmonic (266 nm, ≈ 1 mJ cm^{-2}, 7 ns) of a Nd^{3+}:YAG was used to photolyze the ozone. The second harmonic of another Nd^{3+}:YAG laser pumped a dye laser. The dye laser's second harmonic (≈ 10 μJ cm^{-2}, $\Delta v_{FWHM} \approx 0.3$ cm^{-1}) probed the OH fragments through the (0,0) and (1,1) bands of the $A(^2\Sigma) \leftarrow X(^2\Pi)$ system.[37] The supersonic

expansion and LIF detection apparatus were those used in the ultrafast measurements. In the state-resolved experiments, it was possible to vary the photolysis/probe delay time in 10 ns steps. The signal rose sharply during the initial 20 ns after photolysis, following the integral of the temporal cross-correlation between the photolysis and probe lasers when pulse duration and timing jitter (± 5 ns) are accounted for. The signal remained constant for the next 50–80 ns and then rose slowly or declined slowly, depending on the rovibrational state measured, as a result of collisional relaxation of OH. The data reported here were measured with a 30 ns delay. As in the ultrafast experiments, the LIF signal was linear in both the photolysis and probe laser energy.

The observed spectra were normalized to variations in the photolysis and probe laser fluences and to the intensity of the $P_{11}(15)$, line which was remeasured after scanning 2 nm. The normalized spectra were simulated by Lorentzian line shapes to determine the line intensities of overlapping lines. For hydroxyl in the $A(^2\Sigma)$ state, significant autodissociation occurs for rotational states, $N \geq 25$ in the $v=0$ level and $N \geq 15$ in the $v=1$. All rotational states autodissociate for $v \geq 2$. Because the diagonal bands were probed, only OH($v=0,1$) could be detected. In determining populations from LIF line intensities, we corrected for the fluorescence quantum yield of the specific quantum levels,[38] but do not report populations if the correction was $\geq 50\%$. Division by the Einstein B coefficients[39] converts intensities to relative populations. Results from independent measurements were then averaged.

III. RESULTS

A. Product-state distributions

In order to understand the OH appearance measurements, one must understand the form of the product-state distribution and the extent to which the probe laser spectrum encompasses the absorption spectrum of the product. Figure 3 shows a portion of an OH spectrum following 266 nm photolysis of the $CH_4 \cdot O_3$ cluster. The population distribution, $P_{obs}(v, J, \Omega, \Lambda)$, the probability of OH being formed in a particular quantum state, was derived from the LIF spectra such as that shown in Fig. 3. Hydroxyl has two spin–orbit states[40,41] labeled by the quantum number $\Omega = 1/2, 3/2$. The lower $f_1(^2\Pi_{3/2})$ and the upper $f_2(^2\Pi_{1/2})$ state are separated by 126 cm^{-1} for the lowest rotational level. The splitting decreases with increasing rotational excitation. Each spin–orbit state, in turn, is split into Λ-doublet components, labeled A' and A'', which vary by $\approx 0.2\%$ of the rotational energy for all rotational states probed in this experiment. As N increases, the orbital of the unpaired electron in the A' state becomes localized in the plane of the molecular rotation, while for A'' the electron orbital becomes localized perpendicular to the plane.[40] Because these four unique fine-structure states are not equally populated and the distributions may be related to the reaction mechanism, the population distribution for each state in both $v=0$ and $v=1$ is displayed in Fig. 4.

The populations presented in Fig. 4 agree well with those that we reported earlier.[30] A striking feature of these
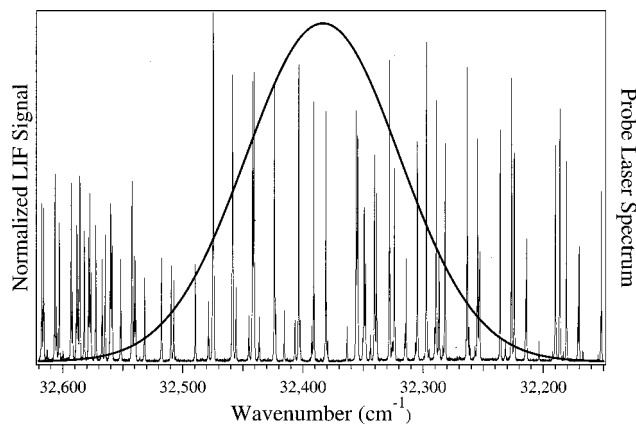
FIG. 3. Shown here is a portion of the LIF spectrum of OH formed following photolysis of the $CH_4 \cdot O_3$ cluster. Superimposed on this LIF spectrum is the power spectrum of the probe laser at 308.8 nm. The strong, low-J, Q and P branch lines and some higher-J levels of the R branch for $v=0$ are probed at 308.8 nm; the $P(N)$ and $Q(N)$ lines decrease in frequency as N increases. The tallest line at 32 475 cm^{-1} is the $Q_{11}(1)$; the doublet at 32 444 cm^{-1} is the overlap of $Q_{11}(2)$ and $P_{11}(1)$; the doublet at 32 355 cm^{-1} is the overlap of $Q_{22}(1)$ and $Q_{11}(7)$.

data is that the f_1 and f_2 levels of the lowest rotational levels are unequally populated, with more population in the f_1 state. One conceivable explanation is that after the reaction the OH has undergone collisions in the beam, with rotational relaxation causing excess population in the states of lowest energy. However, a study of the LIF from these levels as a function of photolysis/probe delay time is consistent with the distributions being unaffected by collisions. Additional tests were performed by moving the laser crossing region from 8
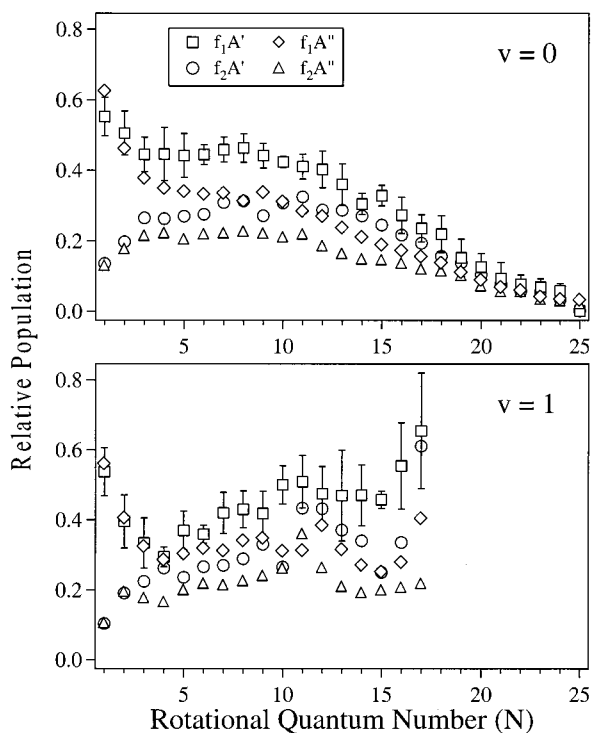
FIG. 4. The OH($v=0,1$) population distributions for each lambda-doublet and spin–orbit state. Both distributions are plotted using the same scale.
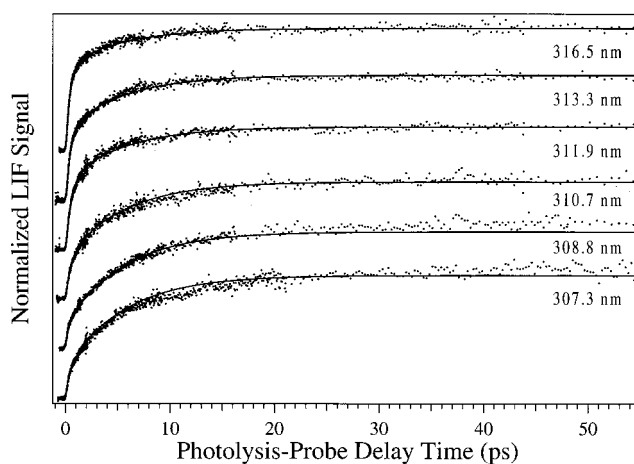
FIG. 5. The dots show the measured OH LIF data for the $CH_4 \cdot O_3$ cluster reaction as a function of photolysis/probe delay time. The asymptotic value was set to unity. The lines represent the optimization of Eq. (5) to the experimental data. The wavelength probed is shown below each appearance curve.

to 20 mm downstream of the expansion nozzle, thereby, reducing the number density and the collision rate by a decade. The populations determined at 20 mm showed no difference from the populations determined at 8 mm. These observations suggest that post-dissociation collisions do not affect the reported $P_{obs}(v,J,\Omega,\Lambda)$. Figure 3 also illustrates how the spectrum of the ultrafast probe laser encompasses many different rovibrational transitions. Superimposed on the state-resolved spectra is a representation of the power spectrum of the probe laser at 308.8 nm, which illustrates that many rovibrational transitions are excited at each ultrafast probe laser wavelength. The shortest wavelengths probe only OH($v=0$). At 307.3 nm, the laser probes many rotational levels, primarily R branch bandheads, of the f_1 and f_2 states. Strong, low-J, Q and P branch lines and some higher-J levels of the R branch are probed at 308.8 nm. When the probe laser is tuned to 310.7 nm, the P and Q branch lines of intermediate-J are probed for f_1 and f_2. The other wavelengths probe a mixture of $v=0$ and $v=1$ levels. The fraction of OH($v=1$) states being probed increases with wavelength, and for probe wavelengths between 308.8 and 316.5 nm, the average internal energy of the OH probed increases uniformly.

B. Time-resolved data

The time evolution of the OH concentration following 267 nm photolysis of the $CH_4 \cdot O_3$ van der Waals complex by an ultrafast laser is shown in Figs. 5 and 6. The signal is plotted as a function of photolysis/probe delay time, t_d, at six different probe wavelengths. Figure 6 shows the early time data on a higher resolution scale. The traces are the averages of eight to ten scans, each of which was acquired during about half an hour. Consecutive scans were acquired from long to short delay time, then from short to long delay time. The data was collected from 1 ps before reaction initiation to 80 ps after reaction initiation. The most striking feature of the data is that both fast (<1 ps) and slow (≈ 5 ps) formation times are obvious in the rise curves. The fraction
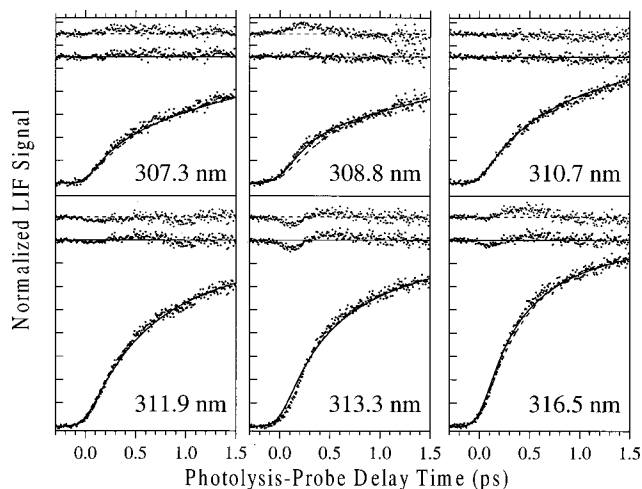
FIG. 6. The dots show the measured OH LIF data for the $CH_4 \cdot O_3$ cluster reaction as a function of photolysis/probe delay time at short time delays. The asymptotic value is set to unity. The dashed lines represent the optimization of Eq. (3), the two-mechanism fit, and the residuals to this fit are shown at the top of each panel. The solid lines represent the optimization of Eq. (5), the three-mechanism fit, to the experimental data, and the residuals to the three-mechanism fit are shown below the two-mechanism residuals. The wavelength probed is given below each appearance curve.

of OH formed with the fast or slow rate depends on probe wavelength. Different wavelengths probe different groups of $OH(v, J, \Omega, \Lambda)$ states; this shows that different $OH(v, J, \Omega, \Lambda)$ levels have different formation rates. The fit of the time- and state-resolved data to particular models is discussed below.

One possibility for different rise times is that the signal arises from more than one reaction product. A number of tests were undertaken to discount this possibility. First, the lifetime of the fluorescence signal was observed to decay by a factor of e^{-1} in ≈ 0.8 μs, which is the lifetime of the OH $A(^2\Sigma)$ state. Furthermore, no signal was detected when the ultrafast probe laser was detuned from the OH $A(^2\Sigma) \leftarrow X(^2\Pi)$ resonance. These observations support attribution of the observed signal to fluorescence from the OH $X \leftarrow A$ transition. Second, the fluorescence signal disappeared if either CH_4 or O_3 was withheld from the plenum. The CH_4 reagent had a stated purity of 99.999%, so an impurity in that gas seems an improbable source of the observed OH. These observations suggest that the observed OH signal arises from a reaction between CH_4 and O. Third, the mole fractions of CH_4 and O_3 were independently varied over an order of magnitude while maintaining a constant backing pressure. While the overall LIF intensity did change linearly with mole fraction, the ratio of fast to slow components and the reaction rate varied by less than five percent, the precision with which the fast-to-slow ratio can be determined from these data. In another test, the mole fraction of CH_4 and O_3 were fixed as the backing pressure was varied from 275 to 345 kPa. Again, the ratio of fast-to-slow components and the reaction rate for each varied by less than five percent. Both of these observations support the idea that the reaction involves the $CH_4 \cdot O_3$ complex, because the density of larger clusters, $(CH_4)_m(O_3)_n$, would be expected to increase rapidly with increasing reagent concentration or plenum pressure. Finally,

almost all of the OH probed on a picosecond-time scale comes from cluster reactions and not subsequent reactive collisions. An upper limit on the OH formation rate, k, from bimolecular collisions can be estimated using the formula

$$k = \rho \sigma_r v, \tag{1}$$

where ρ, the number density of CH_4 in the molecular expansion is $\approx 1.4 \times 10^{16}$ molecules cm^{-3}, the reactive cross section, σ_r, is ≈ 0.20 nm^2, and the relative velocity, v, is $\approx 6 \times 10^4$ cm s^{-1}. These numbers predict a reaction time of ≈ 0.5 μs, about 10^5–10^6 times slower than the rise times reported here. Together, this evidence suggests that the time-resolved data represent the formation rates of OH from the $CH_4 \cdot O_3$ complex.

Comparison of the magnitude of the fluorescence from the cluster photolysis to that from a known pressure of flowing H_2O_2 provides an estimate of the quantum yield of formation of OH from $CH_4 \cdot O_3$. For both experiments

$$LIF = \Phi^{OH} \rho \sigma(\lambda) P_{detect}, \tag{2}$$

where Φ^{OH} is the quantum yield for OH formation, ρ is the density of the reactants, $\sigma(\lambda)$ is the wavelength dependent absorption cross section of the species initiating the reaction and P_{detect} is the probability of detecting the OH formed. The value of these quantities[42–44] for the hydrogen peroxide reaction are $\Phi^{OH} = 1.6$–2.0, $\rho = 10^{15}$ molecules cm^{-3}, and $\sigma(267 \text{ nm}) = 9 \times 10^{-20}$ cm^{-2}. From the known rovibrational distributions of OH, the relative probability of detecting the OH from the two experiments is estimated. For H_2O_2 photolysis, all OH is formed in the $v = 0$, with little (≈ 1050 cm^{-1}) rotational excitation.[45–50] In contrast, for the $CH_4 + O(^1D_2)$ reaction only about a quarter of the OH is formed in the $v = 0$ level,[6] and it is formed with about three times more rotational energy than that from H_2O_2. Because of this difference in the rovibrational distributions, when the ultrafast laser is tuned to 310 nm, a wavelength that probes only OH in $v = 0$ with moderate J, it is ten times more likely to detect an OH from H_2O_2 than an OH from $CH_4 \cdot O_3$. For the $CH_4 \cdot O_3$ reaction, the OH quantum yield is the quantity to be estimated. The absorption cross section[51] for free $O_3 [\sigma(267 \text{ nm}) = 9 \times 10^{-18} \text{ cm}^{-2}]$ should be an adequate estimate of the absorption cross section in the cluster. The density of clusters in the beam was assumed to be $\approx 10\%$ of the O_3 pressure ($\rho \approx 4 \times 10^{14}$ clusters cm^{-3}). This estimate is based on previous studies of the NO dimer in this laboratory[52] showing that a dimer concentration greater than 10% of the monomer produced higher order clusters, causing the signal to become nonlinear (i.e., deviate from the scaling LIF signal$\propto$(NO)$\times$(NO) observed at lower (NO) concentration). The O_3 pressure in our expansion was just below that for which the signal became nonlinear (i.e., deviated from the scaling LIF$\propto$(O_3)$\times$(CH_4)), which we assume indicates a $CH_4 \cdot O_3$ cluster concentration of 10%. The measured signals for both H_2O_2 and $CH_4 \cdot O_3$ photolysis were comparable and from the quantities indicated one estimates the quantum yield for OH production from the cluster to be ≈ 0.4 following 267 nm photolysis. This calculation suggests that the cluster geometry does not impose severe dynamical con-

straints on the reaction. Clearly, this estimate could be in error, since we did not directly measure the concentration of clusters.

IV. DATA ANALYSIS

Above, we saw that the rise time data clearly contained fast and slow components, the ratio of which depended upon the probe wavelength. The time- and state-resolved data are analyzed in this paper with the idea that more than one re-action mechanism produces OH, and that each mechanism has a characteristic formation rate and population distribu-tion. The objective of our analysis is to decompose the ob-served population distribution into a set of distributions, and relate these populations to the measured appearance curves. The product decomposition must be able to predict the frac-tion of population from each mechanism probed at each wavelength in the ultrafast experiments.

A. Time-resolved data

The simplest analysis assumes two unique appearance time constants. The time-resolved data is taken as the sum of two exponentials, so that at each probe wavelength, the LIF time dependence is fit to the following function:

$$\text{LIF}(t_d) = X_\lambda(t_d) \otimes [C_\lambda^f \times \text{OH}_f(t_d) + (1 - C_\lambda^f) \times \text{OH}_s(t_d)] \tag{3}$$

where $X_\lambda(t_d)$ is the measured cross-correlation at photolysis-probe delay time t_d and probe wavelength λ, $\otimes$ denotes con-volution, C_λ^f is the fraction of ''fast'' OH at λ and $(1 - C_\lambda^f)$ is the fraction of ''slow'' OH. The time evolution of the signal also is proportional to the OH number density at time t_d:

$$\text{OH}_f(t_d) = 1 - \text{Exp}(-t_d/\tau_f) \quad \text{and} \tag{4a}$$

$$\text{OH}_s(t_d) = 1 - \text{Exp}(-t_d/\tau_s), \tag{4b}$$

where τ_f and τ_s are the fast and slow appearance time-constants, respectively, and $\text{OH}_{f/s}(t_d) = 0$ for $t_d < 0$. It is as-sumed that the appearance time-constants are fixed, no mat-ter what rovibrational state is produced. However, it is also assumed that both the fast and slow mechanism may contrib-ute to a specific product state. Because the ratio of popula-tion formed by the two mechanisms may be different for each rovibrational state, the value of C_λ^f can be different at each probe wavelength.

All six data sets were fit to Eq. (3) simultaneously by varying the six C_λ^f coefficients, τ_f, and τ_s. The best-fits to the time-resolved data and the associated residuals are dis-played in Fig. 6. The resulting C_λ^f coefficients are shown in Fig. 7 (circles). The fraction of fast OH lies between 0.23 and 0.69, depending on the probe wavelength and thereby the set of rovibrational states being probed. The slow time constant is $\tau_s = 5.5 \, \text{ps} \pm 0.2 \, \text{ps}$ and the fast time constant is $\tau_f = 0.43 \, \text{ps} \pm 0.02 \, \text{ps}$.

The two time-constant fit adequately represents the data, but the residuals in Fig. 6 show that some of the rise times are not exactly fit by two exponentials. To explore whether three exponentials characterize the data better, the appear-ance curves were fit using the function
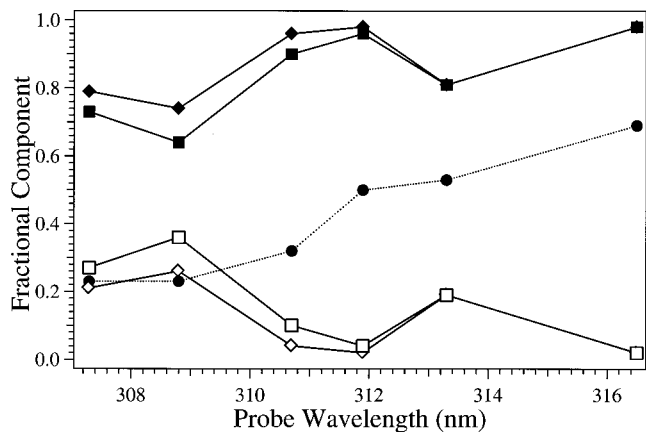
FIG. 7. This figure shows the C_λ^f components, i.e., the fraction of ''fast'' OH determined from the two-mechanism fit [Eq. (3)] of the *time-resolved data* (filled circles) at the six ultrafast probe wavelengths of these experi-ments. Also shown are the components derived from two-mechanism fits of the *product-state data*. The open and closed squares are C_λ^f and $1 - C_\lambda^f$, respectively, using the Boltzmann-based decomposition of the product-state distribution [Eqs. (6) and (10)]. The open and closed diamonds are C_λ^f and $1 - C_\lambda^f$, respectively, using surprisal-based decomposition of the product-state distribution [Eqs. (8) and (10)]. This comparison shows that neither the approach of Eq. (6) nor Eq. (8) gives coefficients close to those extracted from the time-resolved data. The lines connecting the points are to guide the eye.

$$\text{LIF}(t_d) = X_\lambda(t_d) \otimes [C_\lambda^f \times \text{OH}_f(t_d) + C_\lambda^i \\ \times \text{OH}_i(t_d) + C_\lambda^s \times \text{OH}_s(t_d)]. \tag{5}$$

As before $X_\lambda(t_d)$ is the measured photolysis/probe cross-correlation, and C_λ^f, C_λ^i, and C_λ^s are the fractions of the fast, intermediate, and slow channel contributing at λ, which were normalized such that $C_\lambda^f + C_\lambda^i + C_\lambda^s = 1$. Each channel was as-sumed to have a single, exponential rise as shown in Eq. (4). The six data sets were fit simultaneously by varying fifteen parameters: Twelve fractional coefficients and three time constants. The optimized values for C_λ^f, C_λ^i, and C_λ^s are presented in Fig. 8 (open symbols). The three time constants determined are $\tau_\text{fast} \approx 200 \, \text{fs} \pm 70 \, \text{fs}$, $\tau_\text{inter} \approx 500 \, \text{fs} \pm 50 \, \text{fs}$, and $\tau_\text{slow} \approx 5.4 \, \text{ps} \pm 0.3 \, \text{ps}$. Figures 5 and 6 show the fits to the data. The residuals displayed in Fig. 6 show that the three-channel model gives a slightly better fit than the two-state model to the fast rise of the 307.3 and 311.9 nm data and a much better fit to the 308.8 nm data, though the fits at 313.3 and 316.5 nm are not significantly improved.

Fitting to four rate constants did not significantly reduce χ^2 and gave markedly increased uncertainties in the best-fit parameters.

B. State-resolved data

The ultimate objective of this analysis is to relate the observed appearance time-constants to the population distri-bution. In this section, the decomposition of the measured rovibrational distribution is presented. First, different ap-proaches for decomposition of the observed distribution into two distributions are discussed. Then, a three-channel de-composition is presented.
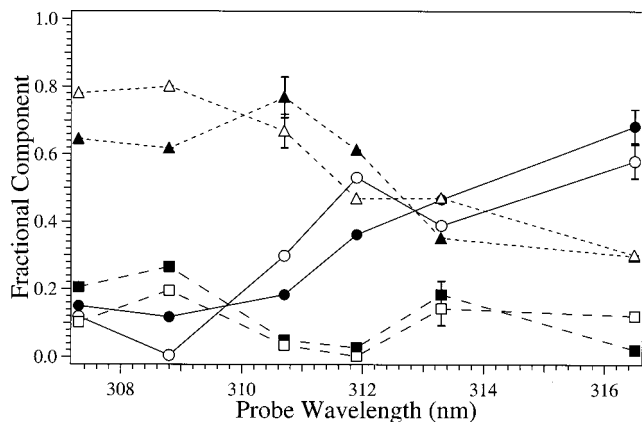
FIG. 8. This figure compares the $C_\lambda^{f/i/s}$ determined from the three-mechanism fitting of time-resolved data [Eq. (5), open symbols] and the $C_\lambda^{f/i/s}$ predicted using the three-mechanism decomposition of the product-state distribution [Eqs. (9) and (10); filled symbols] at the six ultrafast laser probe wavelength used in these experiments. The squares are for the fast time-constant (C_λ^f) and the cold distribution. The circles are the for intermediate time-constant (C_λ^i) and the hot distribution. The triangles are for slow time-constant and the statistical distribution. The lines connecting the points are to guide the eye.

A simple approach is to fit the observed population as the sum of two Boltzmann distributions, $P_{hot}(v,J,\Omega,\Lambda)$ and $P_{cold}(v,J,\Omega,\Lambda)$

$$\frac{P_{obs}(v,J,\Omega,\Lambda)}{2J+1} = C_{hot} \mathrm{Exp}\left(-\frac{E_{rot}}{kT_{hot}}\right)$$
$$+ (1-C_{hot})\mathrm{Exp}\left(-\frac{E_{rot}}{kT_{cold}}\right). \quad (6)$$

A least-squares fit of Eq. (6) to the $v=0$ data gave, $T_{hot} = 4110\,K \pm 106\,K$, $T_{cold} = 156\,K \pm 7\,K$, and $(1-C_{hot})/C_{hot} = 3.5$. For $v=1$, the fit yielded $T_{hot} = 5980\,K \pm 80\,K$, $T_{cold} = 131\,K \pm 6\,K$, and $(1-C_{hot})/C_{hot} = 3.9$. These fit values represent the data well as shown in Fig. 9. The values of $(1-C_{hot})/C_{hot}$ correspond to only 11% of the OH being formed in the cold channel, while 89% is from the hot channel.
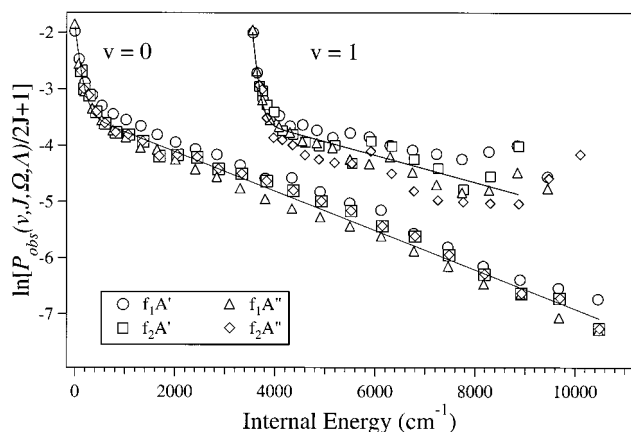
FIG. 9. The symbols show the OH($v=0,1$) rotational population data displayed as a Boltzmann plot. The lines give the two temperature Boltzmann fit via Eq. (6).

Another way to divide the observed population distribution into components is to carry out a surprisal analysis.[53] The rotational surprisal, $I(v,J,\Omega,\Lambda)$, defined as

$$I(v,J,\Omega,\Lambda) = -\ln\left(\frac{P_{obs}(v,J,\Omega,\Lambda)}{P_o(v,J,\Omega,\Lambda)}\right), \quad (7)$$

is calculated as a function of rotational energy. The two reaction mechanisms may have characteristic and distinctly different linear surprisals, aiding in the deconvolution of $P_{obs}(v,J,\Omega,\Lambda)$ into $P_{cold}(v,J,\Omega,\Lambda)$ and $P_{hot}(v,J,\Omega,\Lambda)$. To complete this analysis, the rovibrational prior distribution, $P_o(v,J,\Omega,\Lambda)$, must be computed.

In our calculation of the prior, the production of all quantum states was taken as equally probable, subject only to energy conservation. This distribution would be expected in the absence of any dynamical constraints. The Whitten–Rabinowitz state count was used for the vibrational states and a classical partition function for the CH_3 fragment.[54,55] An exact count was used for the hydroxyl fragment. The prior was then taken as the product of the degeneracy of internal states of both fragments and the translational state density divided by total state density at the energy available to the reaction.[56,57] The prior was calculated for each OH(v,J,Ω,Λ) level individually. The energy available in the reaction was taken to be the sum of the enthalpy of the reaction $CH_4+O(^1D_2)\rightarrow CH_3+OH$ ($15\,240\,cm^{-1}$) and the average translational energy in the center-of-mass frame ($1515\,cm^{-1}$). This number is correct for a free reaction, and using it here assumes that the O_2 generated in the cluster receives the same energy as in the photodissociation of isolated, gaseous O_3. The sum over rotational states, $\Sigma P_o(v,J,\Omega,\Lambda)$ was normalized to $\Sigma P_{obs}(v=0,1;J,\Omega,\Lambda)$ for each vibrational level.

Figure 10 shows the rotational surprisal for OH($v=0,1$) plotted versus the fraction of nonvibrational energy in rotation, $g_r=f_r/(1-f_v)$, where f_r and f_v are the fraction of the total available energy in rotation and vibration, respectively. If $P_{obs}(v,J,\Omega,\Lambda)$ were statistical, the data would fall on a line with a slope of zero. The distribution at low g_r is much colder than the prior distribution, while the distribution at high g_r is hotter than the prior distribution. The surprisal was fit with the equation

$$I(v,J,\Omega,\Lambda) = -\ln\left[\frac{P_{cold}(v,J,\Omega,\Lambda)+P_{hot}(v,J,\Omega,\Lambda)}{P_o(v,J,\Omega,\Lambda)}\right]$$
$$= -\ln[b_{cold}\mathrm{Exp}(m_{cold}g_r)$$
$$+ b_{hot}\mathrm{Exp}(m_{hot}g_r)]. \quad (8)$$

Least squares fits gave $m_{cold}=-128\pm13$, $m_{hot}=2.6\pm0.2$, $b_{cold}=2.53\pm0.38$, and $b_{hot}=0.56\pm0.03$ for $v=0$; for $v=1$, values $m_{cold}=-138\pm18$, $m_{hot}=4.0\pm0.3$, $b_{cold}=3.00\pm0.61$, and $b_{hot}=0.51\pm0.03$ were obtained. The data for $v=0$ and 1 are well fit by the sum of two linear surprisals, as shown by the dashed lines in Fig. 10. Two population distributions, $P_{hot}(v,J,\Omega,\Lambda)$ and $P_{cold}(v,J,\Omega,\Lambda)$, then can be deduced from the surprisal fits.

Last, the rotational surprisals were also fit to three distributions. One will be assumed to be the statistical prior,
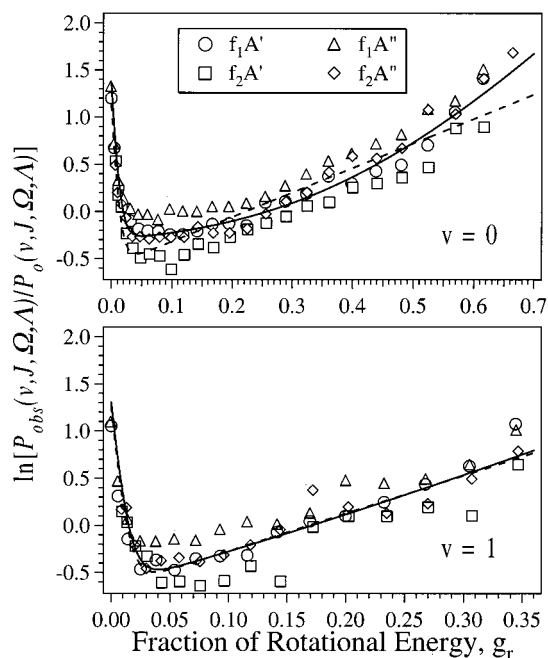
FIG. 10. Surprisal plots for OH($v=0,1$) showing the surprisal as a function of reduced rotational energy, g_r. The dashed lines are the optimization of Eq. (8), the two-mechanism model, to the data. The solid lines are the optimization of Eq. (9), the three-mechanism model.

which is to say the slope of its surprisal is zero. As will be discussed further below, the observation of a component with a slow rise time of ≈ 5 ps suggests that one of the reactive channels produces OH through an CH_3OH^* intermediate in which the energy is randomized. One might reasonably expect the rovibrational energy distribution of the products generated by this channel would be the prior distribution. The surprisal parameters for the other two channels were unconstrained in the fit; one has more rotational energy than the prior and the other less.

Given the aforementioned assumptions, the surprisals were fit using the equation

$$I(v,J,\Omega,\Lambda) = -\ln[b_{cold}\,Exp(m_{cold}g_r) + b_{stat}\,Exp(m_{stat}g_r) + b_{hot}\,Exp(m_{hot}g_r)].$$

(9)

With $m_{stat} \equiv 0$, a least-squares fit to the $v=0$ data in Fig. 10 gave $m_{cold}=-129\pm13$, $m_{hot}=6.0\pm0.5$, $b_{cold}=3.16\pm0.35$, $b_{hot}=0.07\pm0.02$, and $b_{stat}=0.67\pm0.03$. With these values, the population in each of the three distributions may be calculated, giving 12% of the OH($v=0$) created cold, 21% hot, and 67% statistical. The data for the $v=1$ level were fit by assuming the statistical channel has the calculated prior value for the $v=1/v=0$ population (21%); therefore, b_{stat} was set to a fixed value of 0.15. The least-squares fit to the $v=1$ data gave $m_{cold}=-131\pm18$, $m_{hot}=4.7\pm0.3$, $b_{cold}=3.16\pm0.51$, and $b_{hot}=0.38\pm0.02$. This fit gave 11% cold, 74% hot, and 15% statistical for $v=1$. The solid lines in Fig. 10 show these fits to the surprisals. As would be expected, the surprisal data are slightly better fit by the three-distribution model than by the two-distribution model.

The question remains as to which of the alternatives approaches, two appearance time-constants with a two-Boltzmann decomposition of the rotational populations, two time-constants with the two-component surprisal decomposition, or three time-constants with the three-component surprisal decomposition, offers the most consistent explanation of the data.

V. DISCUSSION

A. Comparing alternatives

The principle criterion to be used in assessing which of the alternatives is most consistent with the data will be how well the fractional contributions [$C_\lambda^{f/i/s}$; Eqs. (3) and (5)] determined by fitting the appearance curves are predicted by a given population decomposition. For example, if two reactive channels were operative, we expect the C_λ^f from the appearance curves to agree with the prediction of a two component decomposition of the rovibrational distributions, assuming as usual that different formation times represent different reaction mechanisms and that each mechanism produces a characteristic rovibrational distribution. Below, we consider the two-channel alternatives first, and then turn to the three-channel analysis.

Determining the $C_\lambda^{f/i/s}$ coefficients from the time-resolved date is easy. They are simply the best-fit coefficients of Eqs. (3) and (5). Determining the $C_\lambda^{f/i/s}$ coefficients using the surprisal or Boltzmann decompositions is somewhat cumbersome, because the ultrafast probe laser spectrum encompasses many rovibrational transitions, as illustrated in Fig. 3. However, these coefficients can be calculated by summing over all transitions excited at a particular probe laser wavelength. Specifically, these coefficients can be calculated using the equation

$$C_\lambda^f = \frac{\Sigma[P_{fast}(v,J,\Omega,\Lambda) \times B(v',J';v,J) \times Spec(v',J';v,J)]}{\Sigma[P_{obs}(v,J,\Omega,\Lambda) \times B(v',J';v,J) \times Spec(v',J';v,J)]}.$$

(10)

In this expression, $B(v',J';v,J)$ represents the Einstein B-coefficient for the designated transition; $P_{obs}(v,J,\Omega,\Lambda)$ is the experimentally determined nascent population distribution for OH; $P_{fast}(v,J,\Omega,\Lambda)$ is the population distribution for OH created through the fast mechanism; $Spec(v',J';v,J)$ is the power spectrum of the probe pulse at the excitation frequency; and the sum is over rovibrational states.

These C_λ^f can now be calculated for the two-Boltzmann decomposition of $P_{obs}(v,J,\Omega,\Lambda)$ using the best-fit parameters of Eq. (6) and by associating the $P_{hot}(v,J,\Omega,\Lambda)$ of Eq. (6) with the $P_{fast}(v,J,\Omega,\Lambda)$ of Eq. (10). This association seems intuitive, because for a methanol intermediate one would expect the slower evolving product to be rotationally cooler when compared to the faster evolving product. As Fig. 7 illustrates, the agreement between the time-resolved C_λ^f and the calculated C_λ^f is poor for this product-state decomposition. It is possible, of course, that the association of the $P_{hot}(v,J,\Omega,\Lambda)$ with $P_{fast}(v,J,\Omega,\Lambda)$ is incorrect. If an abstraction reaction were operative, for example, one might expect the fastest mechanism to produce the rotationally coldest product. In this case, the time-resolved C_λ^f would correspond to $(1-C_\lambda^f)$, where the latter C_λ^f is the product-

state prediction. This quantity is also shown in Fig. 7 and also agrees poorly with the time-resolved C_λ^f. This observation is perhaps not surprising, inasmuch as there is no general justification for products having thermal distributions,[58] because the available energy is limited by the sum of the enthalpy for the reaction $CH_4+O_3\rightarrow CH_3+OH+O_2$ and the energy of the photolysis photon.

The comparison can be repeated using the surprisal-based decomposition of $P_{obs}(v,J,\Omega,\Lambda)$. Using the best-fit parameters to Eq. (8), the C_λ^f were again calculated. Again, for a two-mechanism model to be valid, either the calculated C_λ^f or $(1-C_\lambda^f)$ must agree with the best-fit values of the two-exponential appearance model. Again, Fig. 7 shows that agreement is poor.

It appears that the time-resolved and state-resolved data cannot be simultaneously fit with a two-mechanism model. The $P_{obs}(v,J,\Omega,\Lambda)$ data can be decomposed into two unique components. The time-resolved data are adequately fit by the sum of two exponential OH rise times. However, the amplitudes of fast and slow components do not match the amplitudes of the hot and cold distributions for the decompositions considered here. This leaves the three-channel model to be considered.

With the aid of formulas analogous to Eq. (10), coefficients $C_\lambda^{f/i/s}$ for the six probe wavelengths may be calculated from the surprisal analysis and the decomposition of Eq. (9). Figure 8 compares the $C_\lambda^{f/i/s}$ for the three mechanisms that fit the time-resolved data (open symbols) to the $C_\lambda^{f/i/s}$ calculated from the state-resolved data (filled symbols). For all wavelengths, there is close agreement, if the following identification is made: Associate the OH formed fastest with OH formed in the lowest N levels [$\tau_{fast}\approx 0.2$ ps and $P_{cold}(v,J,\Omega,\Lambda)$], the OH formed at the intermediate rate with the hot distribution [$\tau_{inter}\approx 0.5$ ps and $P_{hot}(v,J,\Omega,\Lambda)$], and the OH formed slowest with the statistical channel [$\tau_{slow}\approx 5.4$ ps and $P_{stat}(v,J,\Omega,\Lambda)$]. This three-mechanism model is internally consistent. It must be noted that the three rovibrational distributions are not unique, because there are other distributions with nonlinear surprisals which also fit the data. Improved agreement between the coefficients calculated from time- and state-resolved data can be achieved by varying the fitting parameters slightly from their best fit values. We reiterate that the analysis in terms of three mechanisms arises from our conceptual requirement that each component of $P_{obs}(v,J,\Omega,\Lambda)$ characterized by a linear surprisal must have a unique appearance time-constant and that one of the components of the product-state distribution has a surprisal of zero-slope. The curves in Fig. 11 show the fraction of cold, statistical, and hot product as a function of internal energy calculated from the three-distribution fit parameters. One sees that the cold distribution only contributes significantly to the four, lowest rotational levels. The statistical distribution contributes to the majority of the probed levels, at least for $v=0$, while the hot distribution contributes primarily to OH with an internal energy ≥ 4000 cm^{-1}. Though we have data only for $v=0$ and $v=1$, this model predicts that the statistical mechanism makes a negligible contribution to vibrational levels ≥ 2. If one desires analytic expressions for the three $P(v,J,\Omega,\Lambda)$, one may use the
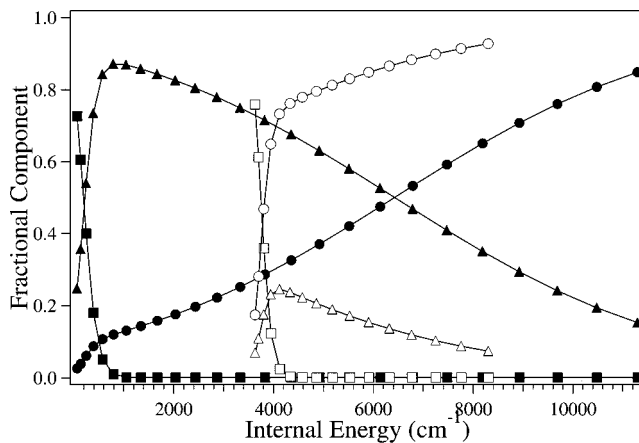
FIG. 11. The fraction of the $OH(v=0,1)$ rotational state populations populated through the three mechanisms: Fast mechanism (squares), dissociation of $[CH_4O]^*$ before complete IVR (circles), and dissociation of a methanol intermediate after IVR (triangles). The fractions were calculated using the best-fit parameters given in the text.

fitting parameters of Eq. (9), e.g., $P_{hot}(v,J,\Omega,\Lambda)$ $= b_{hot} Exp(m_{hot}g_R)/(b_{hot} Exp(m_{hot}g_R)+b_{cold} Exp(m_{cold}g_R)$ $+b_{stat})$ $P_{obs}(v,J,\Omega,\Lambda)$ while using Eq. (6) to represent the values of $P_{obs}(v,J,\Omega,\Lambda)$.

B. Mechanism assignments

The long time constant is almost surely the dissociation of a methanol intermediate after essentially complete IVR according to a statistical theory, such as the Rice–Ramsburger–Kassel–Marcus (RRKM) theory.[59] RRKM rate calculations,[60] consistent with thermal rate coefficients and assuming reasonable values for the CH_3OH^* transition state,[61] fit both the time scale (≈ 10 ns) for dissociation in infrared multiphoton dissociation experiments[62] of the dissociation of CH_3OH and the time scale (≈ 5 ps) for dissociation at the 16 700 cm^{-1} energy in the cluster photolysis experiments. This supports the statistical assignment, because one expects the RRKM rate to scale correctly with internal energy, even though exact agreement is usually achieved only if the transition state is selected to fit a particular microcanonical rate. Statistical adiabatic channel model calculations[63] predict lifetimes of 10 ps for the reaction of thermal $CH_4+O(^1D_2)\rightarrow CH_3OH^*$ at an energy 1300 cm^{-1} less than our hot $O(^1D_2)$ experiments, and 1.6 ps for $O(^1D_2)$ atoms from N_2O photodissociation at 193 nm, providing 7700 cm^{-1} more available energy than in our experiments. These estimates of the lifetime of CH_3OH^* are also in agreement with the value of 5.4 ps observed for the slow component, which is also the slowest rise time measured. No intermediate should dissociate more slowly than that following complete IVR. If IVR is complete within picoseconds—and the contrary would be unexpected at this energy[64]—the longest formation time is, by default, the statistical lifetime. These observations argue for identifying the slow channel with the statistical dissociation of a CH_3OH^* intermediate.

The intermediate formation time of 0.5 ps is ascribed to dissociation of a CH_4O^* intermediate before complete IVR and associated with the high-J fraction of OH arising from

this reaction. According to our three-state decomposition of $P_{obs}(v,J,\Omega,\Lambda)$, this component accounts for about 21% of the population in $v=0$, 74% for $v=1$, and presumably most of the population in $v=2$ to $v=4$. At least three observations bolster this assignment. First, evidence overwhelmingly suggests that $O(^1D_2)$ insertion is the predominant reaction mechanism,[3–7,17,18,24,65,66] pointing to nonstatistical dissociation of CH_4O^*. Second, and related, a 0.5 ps rise time seems too long to be a stripping of a H atom by fast O (forward scattering limit) or a collinear abstraction by fast O (backward scattering limit). The attacking oxygen atom initially moves with an average speed[67] of ≈2.1 nm ps^{-1} and hence would travel the 0.3–0.4 nm necessary for a simple stripping reaction in much less than 0.5 ps. The product OH would presumably gain additional translational energy from the reaction exothermicity, which, in the absence of complex formation, would further decrease the estimated time for a stripping reaction. Last, the OH product is too hot to be the statistical channel. Together, these observations suggest dissociation through a CH_4O^* intermediate before IVR.

The most tenuous part of the present data analysis is the very fast time (0.2 ps) associated with OH in low-J states. This OH accounts for about 11% of the population in both $v=0$ and $v=1$ levels. Fast OH could be formed by O moving perpendicular to a C–H bond and stripping off a H atom at impact parameters sufficiently large to avoid being trapped in the CH_3OH well. Such trajectories presumably would give rise to forward-scattered OH in high, rather than low, rotational states. Collinear attack followed by prompt back-scattered OH could give rise to OH in the low-J levels that seem to be correlated with the shortest time constant. The saddle point on the $O(^1D_2)$ potential surface[16] shows such a collinear C–H–O reaction. Some abstraction component seems consistent with the Doppler spectroscopy results[8–12] which show a slight preference for backward scattering for the OH($v=0,N=5$ and 8). Our decomposition shows that the prompt component contributes mostly to the four lowest f_1 rotational states and predicts that these states would show pronounced backward scattering.

A conceivable explanation for the fast OH in low-J, f_1 levels is reaction of $O(^3P_j)$ formed in about 10% yield in O_3 photolysis with 266 nm light. A large percentage of these atoms have enough energy to surmount the barrier to reaction.[67] Additional $O(^3P_j)$ might also evolve through $O(^1D_2)/O(^3P_j)$ curve crossing in the entrance channel. Because reactions of $O(^3P_j)$ are typically abstractions, the rotationally cold and fast appearing OH may indeed be from reaction with $O(^3P_j)$. On the other hand, low-J, f_1 OH was also preferentially populated in the photolysis of the $CH_4 \cdot N_2O$ cluster,[31] and no $O(^3P_j)$ atoms are formed directly in N_2O photolysis. Also, the low-J population is observed for both the $v=0$ and $v=1$ product, which is different than what has been observed for the reaction between CH_4 and $O(^3P_j)$ where no $v=1$ has been observed. Moreover, *ab initio* calculations of the singlet surfaces do not preclude abstraction trajectories, which would produce rotationally cold products quickly.[16–18] Together, we feel these facts argue against attributing this channel to reaction with $O(^3P_j)$,

though clearly this is not definitive. This alternative is discussed in more detail in the Appendix.

Although our three-mechanism model fits our present data, a crucial question is: Does this model also fit the vast amount of data already available on the $CH_4+O(^1D_2) \rightarrow CH_3+OH$ reaction? If the answer is clearly ''No,'' then it is possible that our data or its interpretation is wrong, or our premise that the cluster reaction is similar to the bimolecular reaction is wrong. This question is systematically addressed in the Appendix, where we compare our data and its interpretation to other experimental and theoretical research on $O+CH_4$. Specifically, we show that our present work is consistent with time scales deduced from chemical quenching experiments, from Doppler spectroscopy, and from angular distributions measured in molecular beam experiments. Our state-resolved measurements are in reasonable agreement with most, but not all, previous gas phase results using several sources of O atoms and different experimental conditions. We show that the $P_{obs}(v,J,\Omega,\Lambda)$ plots of others could be well fit by our three mechanism model, although earlier authors did not do this. The possibility that $O(^3P)$ atoms are significantly influencing the low-N OH in our experiments is examined in detail by reference to theoretical and experimental studies of this specific channel (we argue against it). The influence of the minor channels (e.g., H_2+H_2CO) on our time-dependent results is discussed. The overall conclusion of the Appendix is that our experimental results and the model we use to interpret them are consistent with a great body of data, and that the present approach provides a unifying framework for its understanding. We have put the comparison to previous work, which is extremely important, into an Appendix in order to focus the main part of the paper on our new data and its analysis.

VI. STRENGTHS AND WEAKNESSES OF THE PRESENT EXPERIMENT AND ANALYSIS

Several elements of this experiment and its analysis complicate the interpretation of our results. This section discusses these factors and outlines experimental strategies for circumventing these difficulties.

In these experiments, the appearance rate for most of the product states has not been measured. The free reaction[6] and the cluster reaction[30] between CH_4 and $O(^1D_2)$ produces about half of the OH in vibrational levels $v\geq1$, with $v=2$ the most probable and levels up to $v=4$ populated.[6] The experiment reported here investigated no levels above $v=1$. Moreover, the highest rotational states even for these two vibrational states were not monitored, because of the autodissociation of OH(A). Therefore, the conclusions drawn here are based on probing somewhat less than half the OH product from the reaction. In our preliminary experiments[26] only OH($v=0,J$), formed predominantly through the statistical channel, was probed. As a result, we failed to discover the fast components discussed here. This earlier failure highlights the desirability of obtaining more comprehensive data.

Another limitation of the data presented here is that each appearance curve represents a complicated superposition of many rovibrational states, because of the inherently broad

spectrum of short pulses compared to the spacing of individual OH transitions. This averaging process will tend to obfuscate different appearance rates of specific product states. Although three rise times adequately represented our LIF data within the present signal-to-noise, the idea that there are three distinct OH formation mechanisms, each characterized by a distinct distribution, is presumably overly simple. An absorption experiment could allow measurement of the appearance of individual $OH(v,J,\Omega,\Lambda)$ states. Following photolysis, spectrally broad ultrafast pulses could probe the OH, and a spectrometer could disperse the transmitted light onto a multichannel detector. With this approach, the experimental time resolution is limited by the laser pulse duration, the experimental spectral resolution by the spectrometer, and the observed linewidths by the sample dephasing time.[68] This approach might also permit probing the OH close to the transition state,[69,70] where the $OH(X)$ and $OH(A)$ potentials are perturbed by the CH_3 or O_2 fragments. Such information, combined with sub-Doppler spectra of individual rovibrational states, would yield a more complete picture of the dynamics of this reaction. In the absorption experiment considered above, one would measure the absorption spectrum as a function of time for each $OH(v,J,\Omega,\Lambda)$ state, each of which might have a different and complex time dependence. This approach has previously been used to study photodissociation reactions.[68] Also, an absorption experiment could probe $OH(v>1)$ using strong $A(^2\Sigma) \leftarrow X(^2\Pi)$ absorptions that could not be used in fluorescence due to autodissociation that competes with the 0.8 μs fluorescence lifetime.

The product state distributions were decomposed subject to the condition that one of the three distributions was an unconstrained prior. This restriction was imposed, in part, because infrared multiphoton dissociation studies[62] of CH_3OH showed good agreement between an unconstrained prior and the product state distribution measured in those experiments and between the dissociation rate and RRKM predictions. It should be noted, however, that those experiments were only 2000–3000 cm^{-1} above threshold, while the experiments reported here are $>16\,000$ cm^{-1} above threshold. For reactions without a large barrier, there is evidence that as energy increases, the product-state distributions may become nonstatistical.[71,72] Clearly, if this were true for the CH_3OH^* dissociation, our decomposition of the product-state distribution could be incorrect.

Throughout this paper we compared free and cluster reaction results with the unstated assumption that the reaction mechanisms are similar. However it is important to question whether the trajectories of $O(^1D_2)$ attacking CH_4 in the cluster resemble the trajectories in the free, gas phase reaction. We observed that the OH $v=1/v=0$ ratio for the cluster was the same as for the free reaction and that the rotational state distributions were generally similar [e.g., excluding the lowest N, $T_{rot}(v=0,1) \approx 7000$ K for the bulb reaction and ≈ 5000 K for the cluster reaction][30] As we have discussed before, these observations suggest, but do not prove, that reaction mechanisms in the cluster are similar to those for the free reaction. The $CH_4 \cdot O_3$ cluster environment[73] could have a significant impact on the observed dynamics, and a potential-

energy surface for this van der Waals complex would be helpful. The dissociation of gaseous O_3 has been studied and the dynamics of forming $O(^1D_2)$ and O_2 are fairly well understood. Presumably, complexation does not significantly alter this dissociation process. There is almost complete dissociation within 70 fs.[74–76] While this dissociation is very fast, it is not a negligible fraction of the fastest time-constant measured in these experiments and may limit the time-resolution in these experiments. The average asymptotic velocity[67] of the $O(^1D_2)$ is ≈ 2.1 nm ps^{-1}, directed along the initial O_2–O bond,[77] and the O_2 travels ≈ 1.1 nm ps^{-1}. The O_2 molecule should not alter the long-lived CH_3OH^* dissociation, because the diatom would be on average ≈ 6 nm away from the dissociating methanol. Our RRKM calculations and calculations of the statistical prior energy distributions for the OH and CH_3 products assumed the energetics of the free reaction, i.e., the energy carried by the O_2 molecule was assumed to be unaffected by the complex, an idea which is supported by the similarity between the OH energy distributions for free and cluster reactions.

Since submission of this manuscript, the geometry of a $CH_4 \cdot O_3$ cluster has been determined by another group at NIST,[73] using microwave spectroscopy. This study found the methane moiety to be freely rotating and located atop the ozone molecule. The angle between the line formed by the center-of-mass of the two molecular components and the plane of the ozone molecule was 118.2° and the closest oxygen to carbon internuclear distance was 0.36 nm for the equilibrium structure. If the $O(^1D_2)$ recoils along the O–O bond,[77] it would seem unlikely to react, since the dissociating O is not initially pointed at a H atom; hence this structure seems hard to reconcile with our estimate of a large ($\approx 40\%$) quantum yield for OH formation. However, as noted above, the OH LIF signal scaled with the pressure of the reactants and carrier gases as expected for the $CH_4 \cdot O_3$ complex. Also, the OH rovibrational distributions are similar to the free reaction.[30] These observations strongly suggest that the reaction is taking place in a $CH_4 \cdot O_3$ cluster, rather than some larger $(CH_4)_m \cdot (O_3)_n$ cluster. It is possible that the $CH_4 \cdot O_3$ producing OH in our dynamics experiments has a different geometry from that identified by microwave spectroscopy. Different expansion conditions and apparatus could produce clusters in different geometries. It is also quite possible, as discussed above, that our estimate of a 40% quantum yield is significantly in error due to one assumption we had to make in its derivation. A deep methanol minimum dominates the CH_4–O potential[16–18] and could alter the $O(^1D_2)$ recoil direction, so that reaction occurs despite an unfavorable initial geometry.

In this paper we used complimentary data, product-appearance curves and product-state distributions, to learn about the mechanisms of the elementary reaction $CH_4 + O(^1D_2) \rightarrow CH_3 + OH$, which has rich and interesting dynamics. The data were analyzed under the assumption that each mechanism was characterized by a unique appearance time-constant and that each mechanism produced a unique $OH(v,J,\Omega,\Lambda)$ energy distribution. For the data reported in this manuscript, it was found that a three-channel model (formation times of 0.2, 0.5, and 5.4 ps) best described the data.

An improved experimental approach [e.g., ultrafast ultraviolet absorption rather than LIF] and more comprehensive data would be likely to uncover even more complex reaction dynamics. We hope these studies will motivate a rigorous theoretical investigation of the dynamics of this reaction.

ACKNOWLEDGMENT

APPENDIX: COMPARISON OF THE CH₄·O₃ RESULTS TO PREVIOUS STUDIES OF REACTIVE COLLISIONS BETWEEN CH₄ AND O

As highlighted in the introduction, the literature contains a wealth of information concerning the thermodynamics, chemical kinetics, and molecular dynamics of the reaction between $CH_4+O(^1D_2)$. In this Appendix, we critically compare this literature to our results. The objective of this comparison is to look for evidence in the literature that will test the mechanistic assignment of this paper and to help unify this sizable literature into a comprehensive understanding of the dynamics of the title reaction.

A. Matrix and chemical timing experiments

Much of our intuition about the reactions between atomic oxygen and hydrocarbons is derived from the early work of Cvetanovic and co-workers[66] and DeMore and co-workers.[3–5] Cvetanovic and co-workers[66] proposed three distinct mechanisms: Insertion and fragmentation to form OH, abstraction to form OH, and elimination of molecular hydrogen. In experiments carried out in liquid argon aimed at further elucidating the role of the these proposed mechanisms, DeMore and Raper[4] identified three products for the reaction with methane,

$$CH_4+O(^1D_2) \rightarrow CH_3OH \quad 53\%,$$
$$\rightarrow H_2CO+H_2 \quad 7\%,$$
$$\rightarrow CH_3+OH \quad 40\%.$$
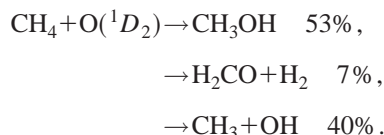
From this work, DeMore[5] speculated that CH₃OH* might be common to all these reaction paths. However, subsequent studies of the free, gas-phase reaction at room temperature lead Lin and DeMore[3] to conclude that about half of the total CH₃ and OH produced passed through a CH₃OH* intermediate, which they estimated to have a lifetime of about 0.8 ps. Production of the other half was attributed to a different prompt mechanism. The production of methyl and hydroxyl radicals at high pressures and even in liquid argon is frequently cited as evidence for an abstraction mechanism that does not involve a methanol-like intermediate. The results of DeMore and co-workers pose two questions. First, is the 0.8 ps consistent with the lifetimes measured in our experiments? Second, does production of methyl and hydroxyl radicals even in liquid argon demand an abstraction channel?

To answer the first question, it is important to understand how the 0.8 ps lifetime was determined. The $O(^1D_2)$ was generated by 184.9 nm photolysis of nitrous oxide, and the translational energy was neither nascent nor fully thermali-

zed. This generation process gave ≈20% uncertainty in the total available energy. The value of 0.8 ps was calculated from the slope-to-intercept ratio (the intercept value being an extrapolation from finite to zero pressures) of a plot of the ratio of the concentration of methanol to the pressure of the cooling gas as a function of methane concentration. While our experiments probe a limited subset of the total product states, the 0.8 ps value is nevertheless similar to the population-weighted average of the rise times that we measured directly. Olzmann[63] has also noted that Lin and DeMore used a strong-collision model in analyzing the chemical timing data, and if one assumes that the collisional cooling rate is different than gas kinetic, a somewhat different lifetime can be extracted from these experiments. Given the experimental uncertainties and differences between the experiments of DeMore and co-workers and the data presented here, we believe that the two lifetime measurements are in remarkable agreement.

To answer whether formation of CH₃ and OH from $CH_4+O(^1D_2)$ in liquid argon requires an abstraction channel, one may compare the vibrational relaxation time of CH₃OH* in liquid argon to the dissociation time of CH₃OH*. The collisional stabilization time, τ_{vr}, can be estimated as

$$\tau_{vr}^{-1}=k_{vr}\rho g(r). \tag{A1}$$

In this expression, k_{vr} represents the vibrational relaxation rate constant of CH₃OH* in liquid argon at a temperature of 87 K, ρ is the density of the liquid argon, and $g(r)$ is the radial distribution function evaluated at the Lennard-Jones diameter.[78] The exact value for k_{vr} is not known, but it is likely to be slightly less than the gas kinetic rate, and we assume it to be $\approx 10^{-10} \, cm^3 \, s^{-1}$. The argon density is $\approx 2.3 \times 10^{22} \, cm^{-3}$. The value of the radial distribution is also unknown, though in general it lies between 1 and 3, and we will take a value of 2. Using these numbers in the Eq. (A1) gives a $\tau_{vr} \approx 0.2 \, ps$. If we take the dissociation time, τ, to be 0.5 ps (the dissociation time we have assigned to the incomplete IVR mechanism), then the probability of the intermediate dissociating prior to vibrational relaxation is $1-\exp(-\tau_{vr}/\tau) \approx 0.33$. That is, one-third of the CH₃OH* would have dissociated into CH₃ and OH prior to stabilization of CH₃OH*. This number lies very close to 40% reported for the reaction in liquid Ar. This estimate suggests that the collision stabilization of CH₃OH*, even in liquid argon, is unlikely to be much faster than the rate of OH formation. Therefore, observation of OH does not necessarily suggest an abstraction mechanism against an insertion/elimination mechanism. It should be noted that photolysis of O₃–CH₄ mixtures in solid argon at 20 K reportedly gives only CH₃OH.[79] This may be because IVR is faster in solid than liquid argon, or more likely, that the fragments are trapped so that geminate recombination occurs.

B. State-resolved measurements

In his pioneering studies of this reaction, Luntz[7] photolyzed ozone at 266 nm in a dilute gaseous Ar–O₃–CH₄ mixture and probed OH($v=0,1$). The experiments were carried out at a density of $6 \times 10^{16} \, cm^{-3}$ and a photolysis/probe time

delay of 0.5 μs, presumably ensuring that the hot oxygen atoms formed in the photolysis were thermalized prior to reaction. As a result of this thermalization, the O($^1D_2$) carried $\approx$1200 cm^{-1} less energy; moreover, the O(^3P_j) atoms lacked sufficient translational energy to surmount the barrier for reaction. However, the long photolysis/probe delay and the relatively high pressures opened the possibility of collisional relaxation of OH(v,J,Ω,Λ) that would alter the nascent distribution, though Luntz maintained that the distributions were close to nascent. Luntz reported that $v=0$ and $v=1$ were comparably populated and had similar rotational state distributions. The f_1 and f_2 spin–orbit states were equally populated, and the Λ-doublet ratio increased from unity at low-N to $\approx$1.7 at $N=19$. A surprisal analysis was done for the rotational distribution. Luntz decomposed this surprisal into two regions. Levels for $N>6$ were well fit by a line of slope $\approx$6.5, whereas states for $N<6$ were much colder, and deviated greatly from a linear surprisal. From the data in Luntz's Fig. 2, the cold component can be estimated to be $\approx$7% of the total population. The $P_{obs}(v,J,\Omega,\Lambda)$ peaks at $g_r\approx$0.3. Luntz attributed the population characterized by the linear surprisal as product from a CH$_3$OH* intermediate before complete IVR. The minor, cold OH was from an in-line collision at low impact parameter giving rotationally unexcited product. Our analysis of the data from these experiments is consonant with his interpretation of the distribution for high-N. However, we believe there is a significant contribution from a statistical channel that contributes to OH at both intermediate- and low-N, which would be identified if our three-mechanism model were used to analyze Luntz's data.

In a similar set of experiments, Park and Wiesenfeld[6] (PW) probed OH($v=0,1,2,3,4$) following 248 nm photolysis of ozone in a Ne–CH$_4$–O$_3$ mixture. A density of 5 $\times10^{15}$ cm^{-3} and a delay time of 0.2 μs were used, which should make the $P_{obs}(v,J,\Omega,\Lambda)$ close to nascent, though the cooling of the hot O(^3P_j) before a reactive collision would be incomplete. The fractional population in vibrational levels $v=0–4$ was reported to be 0.25, 0.25, 0.33, 0.12, and 0.05, respectively. These vibrational populations are in fair agreement with those from an infrared chemiluminescence study[80] (which could not probe $v=0$) and a LIF study that probed rotationally relaxed OH($v=0,1,2$).[81] PW found that a rotational temperature of $\approx$7000 K characterizes $P_{obs}(v=0,J,\Omega,\Lambda)$ well within the range 1000–10 000 cm^{-1}. At lower-N, a second, almost thermal component was observed, though PW did not give a characteristic temperature. They reported near-equal population of the two spin–orbit states and an average A'/A'' ratio of $\approx$1.6, which increased with N. Both the $v=0$ and $v=1$ surprisals were linear between g_r of 0.17 and 0.7, with a slope of $\approx$5.5. The surprisal of the $v=0$ data, shown in Fig. 12 of their paper, is linear with a slope near zero for rotational levels $g_r<$0.17. PW interpret the high-N population producing the linear surprisal as arising from insertion and elimination before energy randomization. The colder OH was ascribed to dissociation of CH$_3$OH* after energy randomization. PW reported that fraction of the rotational population arising from this second channel to be 18% and 6% for $v=0$ and $v=1$, respectively. It appears the

PW $v=0$ data for states with internal energies $<$3000 cm^{-1} lie very close to a linear surprisal with zero-slope. It is likely that if the PW data were analyzed by the three state model above (one channel to be characterized by an unconstrained prior), a statistical channel greater than 18% would be deduced.

Wada and Obi (WO) have reported $P_{obs}(v=0,1;J,\Omega,\Lambda)$ of OH from CH$_4$+O($^1D_2$) both for the free reaction and for the CH$_4\cdot$N$_2$O cluster.[31] Photolysis of N$_2$O at 193 nm produced O($^1D_2$) with an average total energy for the reaction of about 18 400 cm^{-1}. For the free reaction, a $v=1/v=0$ ratio of 1.1 was measured. For both $v=0$ and $v=1$ the high-N levels are characterized by a temperature of $\approx$13 000 K and for the low-N states a temperature of $\approx$1000 K. WO found the average f_1/f_2 ratio to be 1.1 for $v=0$ and $v=1$. The average value of A'/A'' was 1.9 for $v=0$ and 1.3 for $v=1$. For the cluster reaction, they found the same $v=1/v=0$ ratio and comparable rotational distributions and A'/A'' ratios. Notably, the f_1/f_2 ratio at low N was larger for the cluster than for the free reaction and resembles the CH$_4\cdot$O$_3$ cluster data in Fig. 4. The high-N cluster data gave a linear surprisal, with a slope of 6.9 for both $v=0$ and $v=1$. They deduce the cold, low-N population to be 24% of the total for $v=0$ and 7% for $v=1$ for the cluster, and 16% and 5% for the free reaction. They assigned the colder OH to the dissociation of CH$_3$OH* after complete energy redistribution and the hotter, high-N to insertion of O($^1D_2$), followed by dissociation prior to complete IVR. González et al.[18] have also measured the rovibrational distribution of the OH fragment using 193 nm photolysis of N$_2$O, and report very similar distributions for the free reaction.

The WO fits to their $P_{obs}(v,J,\Omega,\Lambda)$ results are quantitatively different from our results, although we believe that different approaches to data analysis account for some of the apparent discrepancy. WO give much hotter values for the rotational temperature at high-N (13 000 K compared to our result of 4100 K for $v=0$ and 6000 K for $v=1$). The differences seem greater than can be accounted for by the 11% higher available energy in the CH$_4\cdot$N$_2$O photolysis. However, while the WO data for the $v=1$ level has a great deal of scatter, it does appears to overlap our $v=1$ $P_{obs}(v,J,\Omega,\Lambda)$ plots almost exactly. Perhaps some difference in the temperature determinations accounts for these apparent differences, or perhaps the derived values overlap within the associated uncertainties. The value of the surprisal slope of 6.9 may be compared to our value of 5.5 in our three-state fit. It appears from WO's Fig. 6 that much of the data for $g_r<$0.2 could be fit by a linear surprisal of slope zero. It is likely that if the WO data were analyzed using a three state model, a statistical channel greater than 24% for $v=0$ and 5% for $v=1$ would be deduced, bringing their conclusions closer to ours.

Naaman and co-workers[82,83] measured $P_{obs}(v,J,\Omega,\Lambda)$ after initiating the reaction by 266 nm photolysis of O$_3$ in a crossed beam experiment. The rotational distribution for $v=0$ and $v=1$ were reported for $N<14$. For $v=0$, these distributions are hotter than our cluster results and cooler than those of PW. An f_1/f_2 ratio of $\approx$2.4 and $\approx$1.3 was reported for the low-N levels of $v=0$ and $v=1$, respectively; other

rotational levels appear to have ratios near unity. The authors stated that there is a slight preference for the f_1 spin–orbit state after correcting for the $2J+1=N/N+1$ statistical weight. Naaman and co-workers report that the A'/A'' ratio for OH($v=1$) increases from ≈ 2 to ≈ 10 between $N=1-13$. This unusually large propensity of the A' state was attributed to the cold temperatures of the beam. A similar propensity has not been observed in reactions initiated in van der Waals clusters, where one might reasonably presume the rotational temperature of reactants to be comparable to those in a crossed beam experiment. The OH velocity distribution was also measured in the crossed-beam experiments and reported to have an average value of $\approx 6 \times 10^5$ cm s^{-1}. Because this value would correspond to a total translational energy release to both fragments of about 60 000 cm^{-1}, as compared to $\approx 22 100$ cm^{-1} available, we presume it to be incorrect. In any event, the rotational distribution at low-N, spin–orbit ratio, Λ-doublet ratio, and velocity distribution reported for these crossed beam experiments are quite different from the results reported by Luntz,[7] Park and Wiesenfeld,[6] Wada and Obi,[31] and our laboratory.[30] Indeed, there is a strong congruence in this latter group of experiments. The surprising uniqueness in the data reported by Naaman and co-workers perhaps suggests that there are not-yet-understood differences between the data from the molecular beam environment and the cluster *and* gas cell environments.

C. Doppler spectroscopy

Simons and colleagues have studied the free reaction between CH$_4$+O($^1D_2$) using Doppler spectroscopy.[8–12] These investigations probed OH($v=0,N=5,8,19$) and the very minor product OH(4, 8). The O($^1D_2$) in the Doppler experiments was from photolysis of N$_2$O at 193 nm and, as noted above, the reaction had substantially more translational energy than experiments using ozone photolysis. Nevertheless, this is still small compared to the reaction enthalpy and probably changes the lifetime of the statistical channel only slightly, though it is difficult to assess how the changed collision energy might alter the lifetime of the nonstatistical channels.

Two conclusions from these Doppler profiles pertain to our experiments. First, for OH($0,5,f_1,A'$ and A'') and OH($0,8,f_1,A'$) Doppler profiles showed the average translational energy was about a quarter of the available energy [cf. Figs. 1(d), 2(d), and 3(d) of Ref. 8]. The observed fraction of energy in translations compares well to 20% predicted by our prior calculations described above. Second, the differential scattering cross sections deduced from the detailed shape of the Doppler profiles OH(0,19) showed backwards scattering,[10] with the most probable center-of-mass scattering angle of 115° with a FWHM of 70°. Similarly, for OH($v=0,N=5,8$) about a quarter to one-third of the product was scattered backward in a 40° cone about the line-of-impact (cf. Figs. 2 and 3 of Ref. 8). Neither of these scattering patterns is what would be expected for a long-lived complex.

In the Doppler experiments ''long-lived'' means with

respect to the rotational time of the complex forming the OH state probed. To reconcile the asymmetry in the differential scattering cross sections to our earlier report of only long-lived statistical formation of OH($v=0$), Simons and co-workers postulated a correlation between the impact parameter (the rotational period of the CH$_3$OH* intermediate is inversely proportional to the impact parameter) and scattering angle. Indeed, such a correlation may be associated with distinct mechanisms we have identified. In light of our present findings, however, it is likely that at least two reaction mechanisms contribute to each of the OH($v=0,N$), so the observed distribution would be a superposition of an asymmetrical scattering distribution from a short-lived component and a symmetric distribution from the statistical channel. Our deconvolution of the population distribution into three components allows us to estimate that for the OH($v=0,N=5,8$) levels about 80% of the population was from the statistical channel, and about 20% from the intermediate channel (cf. Fig. 11), which is comparable to the fraction back-scattering products deduced from Doppler profiles.

D. Theory

Arai, Kato, and Koda have calculated potential-energy surfaces for CH$_4$–O(^1D), subject to some geometrical restrictions.[16] The minimum energy path for the reaction travels along a narrow valley, with the O atom collinearly approaching the C–H bond, to a saddle-point with a collinear C–H–O structure. At this saddle-point the C–H bond length (110 pm) is close to the CH$_4$ equilibrium value, and the OH bond length is 166 pm, as compared to 97 pm for OH(X). The electronic energy of the saddle-point is only slightly higher than the separated reactants. From this transition state, the minimum energy path leads directly to CH$_3$OH in its equilibrium geometry. The exit channel leading to CH$_3$+OH is broad and extends nearly up to the saddle point. This observation lead Arai *et al.*[16] to suggest that the reaction might proceed through abstraction-like trajectories directly from the saddle-point without ever passing through a methanol-like geometry.

González *et al.*[18] have recently calculated another *ab initio* potential. They fit this potential, treating the methyl moiety as a pseudoatom. This parameterized potential was then used to run quasiclassical trajectory calculations for several collision energies.[17,18] The calculated OH rovibrational distribution was found to be in good agreement with the measured distributions.[6,18,31] At a collision energy of 1710 cm^{-1} (0.212 eV, corresponding to O($^1D_2$) from photolysis of ozone), all reactive trajectories involved insertion into a C–H bond. There were, however, two classes of these trajectories. One of these was a direct mechanism. The CH$_3$OH* intermediate had a negligible lifetime. The OH rovibrational distribution for these trajectories was inverted, with $v=2$ being the most probable state. The other class involved a CH$_3$OH* intermediate that existed for several vibrational periods. The lifetime of this intermediate ranged from 40 fs to 2 ps, with 0.2 ps being the average value.[17] The rovibrational distribution arising from these trajectories was not inverted, and $v=0$ was the most probable vibrational state. There was es-

sentially equal probably for a trajectory to be direct or indirect. A small but clear dependence of the lifetime of the intermediate was observed with varying collision energy,[18] and the rovibrational distributions changed with changing collision energy. While less than 1% of the total number of reactive trajectories at 1710 cm^{-1}, abstraction-like trajectories were observed, and contributed to 8.3% of all trajectories at 6450 cm^{-1} (0.8 eV). It is important to note that the lifetimes obtained in these calculations are probably lower limits. By treating the methyl moiety as an atom, many vibrational modes are eliminated and presumably these extra degrees of freedom into which energy could flow would tend to slow the reaction time. Despite the imperfect agreement between the appearance times measured in these experiments and the reaction times from these calculation, it is suggestive that an insertion complex was seen to give product on two distinct time scales and that there were a few abstraction trajectories. This finding is not unlike what is reported here.

E. The reaction of $CH_4 + O(^3P_j)$

Because ozone photolysis near 266 nm has a $O(^3P_j)$ quantum yield[67] of $\approx 10\%$, the possibility of $O(^3P_j)$ reactions must be considered. A high barrier (3300–3600 cm^{-1}) to the reaction of $O(^3P_j)$ with CH_4 exists so substantial energy is necessary to promote this slightly endothermic reaction[2] ($\Delta H_{0K}^o = 7.5$ kJ mol$^{-1} = 630$ cm^{-1}). The distribution of translational energy in the $O(^3P_j)$ generated by ozone photolysis is broad,[67] but most atoms carry enough translational energy to overcome the barrier. On average there is ≈ 6400 cm^{-1} of translational energy available in the $O(^3P_j)$–CH_4 center-of-mass frame. To assess whether $O(^3P_j)$ reactions are contributing to the time-resolved measurements reported here, we turn to what is known about the free, bimolecular reaction between $O(^3P_j)$ and methane.

The rovibrational energy distribution in the hydroxyl product has been measured, and the potential surface of the $O(^3P_j)$ has been extensively studied. The most recent and comprehensive of these experiments used $O(^3P_j)$ generated by photolysis of NO_2 to study the reaction with methane.[84] The translational energy distribution of the $O(^3P_j)$ generated is broad,[85] and the most-probable translational energy is ≈ 9990 cm^{-1}, giving about ≈ 4900 cm^{-1} of available energy in the CH_4–$O(^3P_j)$ frame. For methane, the rotational distribution may be roughly characterized by a temperature between 800 and 1100 K. The $OH(v=0,N=1-7,f_1)$ states were found to have an average rotational energy of 580 cm^{-1}, $\approx 12\%$ of the available energy. No $OH(v=1)$ could be detected and the rotational-state averaged Λ-doublet ratio was reported to be near unity. The $f_1/f_2 \times (N/N+1)$ ratio varied between 1.5 and 2 for $OH(v=0, N<5)$. It has often been suggested that the origin of the high spin–orbit ratio points to an adiabatic reaction co-ordinate, inasmuch as only specific spin states (j) correlate to particular OH spin–orbit levels. However, strict adiabatic correlation gives a spin–orbit ratio larger than observed. This lead to the conclusion that a combination of angular momentum mixing in the entrance channel and spin–orbit coupling in the exit channel is the best explanation for the observed f_1/f_2 ratio.[86]

All theoretical calculations[87–90] have found the minimum energy path has a high barrier along the O–H–CH$_3$ co-ordinate, and the minimum-energy configuration atop the barrier is a collinear C–H–O geometry. At this transition state, however, a 20° bend of the C–H–O angle costs only ≈ 350 cm^{-1}, which makes this potential more like a funnel than a tunnel.[89]

Let us now compare what is known about the reaction $CH_4 + O(^3P_j) \rightarrow CH_3 + OH$ and the cold and fast OH observed in these experiments. The two-Boltzmann fit to our data gave a $OH(v=0,$ low-$N)$ distribution characterized by ≈ 150 K; and the three-channel model, the average energy for $OH(v=0,f_1)$ for the cold distribution is 86 cm^{-1}, corresponding to only 2% of the available energy. This distribution is significantly colder than the measured and calculated distribution for reaction with $O(^3P_j)$. However, the energy available in both experiments is both uncertain and broad, and this difference might reflect different energetics. More importantly, we observe this preferential population of the f_1 level both in $v=0$ and $v=1$, and the fractional population attributed to the fast/cold mechanism is the same ($\approx 11\%$) for both vibrational levels. This contrasts with the experiment and theoretical finding that reaction with $O(^3P_j)$ gives little population in $v>0$. Another point worth noting is that in the $CH_4 \cdot N_2O$ cluster experiments—but not in the cell experiments using N_2O—a high f_1/f_2 ratio for low-N was also observed, and $O(^3P_j)$ is not produced in the photolysis of N_2O.

For the data presented here, the preferential population of f_1 at low-J could arise from reaction of nascent $O(^3P_j)$ formed in the photolysis of ozone. However, the observation that the rotational distribution is much colder than that for reaction with $O(^3P_j)$, the observation that this component is in both $v=0$ and $v=1$, and the observation that a similar cold component for reactions in the $CH_4 \cdot N_2O$ cluster suggests to us that this population does not arise from an $O(^3P_j)$ reaction. It might also be possible that the unusually large population in low-J f_1 states is an effect unique to the cluster, perhaps involving the adjacent N_2 or O_2 molecule, an orientation effect of the reactants in the cluster, or a curve-crossing.

F. Other channels

Although formation of $CH_3 + OH$ is the primary channel in the bimolecular reaction between $CH_4 + O(^1D_2)$, it is not the only channel. The reported contributions of the various channels have varied greatly. For example, estimates of the contribution of the principal channel have spanned 69%–96%. Lee and co-workers[23] recently critically reviewed the work of Hack and Theismann,[24] Brownsword et al.,[19] Satyapal et al.,[21] and their own crossed-beam experiments[22,23,91] and recommend the branching ratios listed below, which are given along with the standard enthalpies of reaction at 0 K.

$$CH_4 + O(^1D_2) \rightarrow CH_3 + OH \qquad\qquad 69\% \qquad -182 \text{ kJ mol}^{-1}$$

$$\rightarrow CH_2OH + H \qquad\qquad\qquad\qquad\qquad -165 \text{ kJ mol}^{-1}$$

$$\text{or} \qquad\qquad\qquad\quad \Big\} \quad 23\%$$

$$\rightarrow CH_3O + H \qquad\qquad\qquad\qquad\qquad -129 \text{ kJ mol}^{-1}$$

$$\rightarrow H_2CO + H_2 \qquad\qquad\qquad\qquad\qquad -482 \text{ kJ mol}^{-1}$$

$$\text{or} \qquad\qquad\qquad\quad \Big\} \quad 5\%$$

$$\rightarrow HCOH + H_2 \qquad\qquad\qquad\qquad\qquad -255 \text{ kJ mol}^{-1}$$

$$\rightarrow CH_2(\tilde{a}\,^1A_1) + H_2O \qquad 1.5\% \qquad -179 \text{ kJ mol}^{-1}$$

$$\rightarrow CH_4 + O(^3P_j) \qquad\qquad 1.5\% \qquad -190 \text{ kJ mol}^{-1}$$
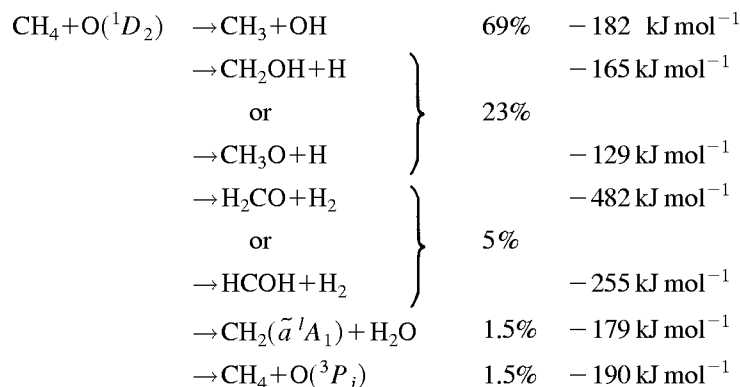
This overview shows not only that there are several competitive channels, but also that production of $CH_3 + OH$ is not the lowest energy channel. This is also illustrated in Fig. 1, which is based on the best experimental data and theoretical calculations presently available.[2,89,92–96] Figure 1 illustrates that one reason the lower energy products are not favored is the presence of significant potential-energy barriers separating the methanol well from these lower energy asymptotes.

Lee and co-workers[22,23] also studied the atomic and molecular hydrogen channels in crossed molecular beams. They found that the H_2 product was isotropically distributed, suggesting that this channel is likely to be formed in a statistical process. For the atomic hydrogen channel about 90% of the product was isotropically spread, which again supports an intermediate in which energy is randomized prior to dissociation. However, the remaining 10% was back scattered, suggesting that a fast mechanism operates in parallel. They also concluded that the partner species for this channel was more likely to be hydroxymethyl (CH_2OH) rather than the methoxy radical (CH_3O). This finding further provides evidence for a long-lived intermediate, because although the former is ≈ 36 kJ mol^{-1} lower in energy than the latter, to form CH_2OH the CH_3OH^* complex must live long enough for energy to migrate to the C–H bond. Satyapal et al.[21] measured Doppler spectra of the H atom. They measured that about 20%–23% of the available energy appears in translation. They also concluded from comparing H atoms for photolysis of methanol and Doppler spectra of nascent H from reaction of $CH_4 + O(^1D_2)$, that an intermediate existed. Satyapal et al.[21] estimated that its lifetime was ≈ 0.8 ps. This lifetime is commensurate with the 0.5 ps that we have assigned to the dissociation of a CH_4O^* intermediate. While it is clear that further studies will be needed to fully elucidate the dynamics of these minor channels, the data support our identification of an intermediate species following insertion as the principle mechanism.

Evidence suggests that a CH_3OH^* intermediate dissociates to form $CH_2OH + H$, $CH_3 + OH$, $H_2CO + H_2$, and $CH_2(\tilde{a}) + H_2O$, which begs the question of whether the quantum yields are consistent with this idea. Our results suggest that 67% of OH($v = 0$), 15% of OH($v = 1$), and 3% of OH($v = 2$) are formed by decay of such an intermediate. These percentages and the measured ratios[6] ($v = 0)/(1)/(2) = 0.25/0.25/0.33$ imply that $\approx 21\%$ of the total

OH is formed via the RRKM intermediate. Therefore, $0.69 \times 0.21 \approx 14\%$ of the total reactive collisions result in formation of CH_3OH^* followed by statistical dissociation to $CH_3 + OH$. According to work mentioned in the preceding paragraph,[23] 23% of the reactive scattering gives $CH_2OH + H$, of which 90% is isotropically scattered, representing decay of a long-lived intermediate. This implies that $\approx 21\%$ of reactive collisions result in formation of CH_3OH^* followed by statistical dissociation to $CH_2OH + H$. An additional 5% is ascribed to $CH_3OH^* \rightarrow H_2CO + H_2$, and 1.5% to $CH_3OH^* \rightarrow CH_2(\tilde{a}) + H_2O$. Is the decay of CH_3OH^* into these four channels in the ratio 14/21/5/1.5 reasonable? One expects loose, barrierless transition states for the two simple bond-breaking channels. The $CH_3 + OH$ channel is favored by a slightly lower energy than $CH_2OH + H$, and one expects it to be $\approx 50\%$ faster on that basis. However, the latter channel is triply degenerate, favoring it by a factor of 3. The net expectation for decay of CH_3OH^* is close to the 14/21 ratio deduced from the experiments. The $CH_2(\tilde{a}) + H_2O$ channel, although essentially isoenergetic with the OH channel, appears to require an unlikely transition state (low Arrhenius A-factor), resulting in its much lower branching ratio. Presumably this is also the reason for the low yield of H_2, despite its being much lower in energy than the other three channels. Therefore, one may plausibly ascribe the indicated fractions of these four different reactions to statistical decay of a CH_3OH^* intermediate. An implication of this is that the slow OH formation time we determined ($\tau_{slow} \approx 5.4$ ps ± 0.3 ps) is the total decay time of the CH_3OH^* precursor to the four reactive channels. One would predict that if H, $CH_2(\tilde{a})$, or H_2, were probed, the same 5.4 ps formation time would be found. If so, then the identification could be made: $k_{uni} = (5.4 \text{ ps})^{-1} = k(OH) + k(H) + k(CH_2(\tilde{a})) + k(H_2)$, where the ratio of unimolecular rate constants (at $\approx 50\,000$ cm^{-1} in the CH_3OH^*) is in the ratio 14/21/5/1.5 deduced above.

[1] N. Basco and R. G. W. Norrish, Proc. R. Soc. London, Ser. A **260**, 293 (1961).
[2] *NIST-JANAF Thermochemical Tables*, 4th ed., edited by Malcolm W. Chase, Jr. (ACS/AIP, New York, 1998).
[3] C.-L. Lin and W. B. DeMore, J. Phys. Chem. **77**, 863 (1973).
[4] W. B. DeMore and O. F. Raper, J. Chem. Phys. **46**, 2500 (1967).
[5] W. B. DeMore, J. Phys. Chem. **73**, 391 (1969).
[6] C. R. Park and J. R. Wiesenfeld, J. Chem. Phys. **95**, 8166 (1991).
[7] A. C. Luntz, J. Chem. Phys. **73**, 1143 (1980).

[8] M. Brouard, H. M. Lambert, C. L. Russell, J. Short, and J. P. Simons, Faraday Discuss. **102**, 1 (1995).

[9] M. Brouard, H. M. Lambert, J. Short, and J. P. Simons, J. Phys. Chem. **99**, 13571 (1995).

[10] M. Brouard, S. P. Duxon, and J. P. Simons, Isr. J. Chem. **34**, 67 (1993).

[11] J. P. Simons, J. Chem. Soc., Faraday Trans. **93**, 4095 (1997).

[12] M. Brouard, S. P. Duxon, P. A. Enriquez, and J. P. Simons, J. Chem. Soc., Faraday Trans. **89**, 1435 (1993).

[13] T. Suzuki and E. Hirota, J. Chem. Phys. **98**, 2387 (1992).

[14] R. Schott, J. Schlutter, M. Olzmann, and K. Kleinermanns, J. Chem. Phys. **102**, 8371 (1995).

[15] J. Schlutter, R. Schott, and K. Kleinermanns, Chem. Phys. Lett. **213**, 262 (1993).

[16] H. Arai, S. Kato, and S. Koda, J. Phys. Chem. **98**, 12 (1993).

[17] M. González, J. Hernando, I. Baños, and R. Sayós, J. Chem. Phys. **111**, 8913 (1999).

[18] M. González, M. P. Puyuelo, J. Hernando, R. Sayós, P. A. Enríquez, J. Guallar, and I. Baños, J. Phys. Chem. A **104**, 521 (2000).

[19] R. A. Brownsword, M. Hillenkamp, P. Schmiechen, and H.-R. Volpp, J. Phys. Chem. **102**, 4438 (1998).

[20] Y. Matsumi, K. Tonokura, Y. Inagaki, and M. Kawasaki, J. Phys. Chem. **97**, 6816 (1993).

[21] S. Satyapal, J. Park, R. Bersohn, and B. Katz, J. Chem. Phys. **91**, 6873 (1989).

[22] J. J. Lin, Y. T. Lee, and X. Yang, J. Chem. Phys. **109**, 2975 (1998).

[23] J. J. Lin, S. Harich, Y. T. Lee, and X. Yang, J. Chem. Phys. **110**, 10821 (1999).

[24] W. Hack and H. Thiesemann, J. Phys. Chem. **48**, 17364 (1995).

[25] W. Hack, H. Gg. Wagner, and A. Wilms, Ber. Bunsenges. Phys. Chem. **92**, 620 (1988).

[26] R. D. van Zee and J. C. Stephenson, J. Chem. Phys. **102**, 6946 (1995).

[27] C. Jacques, L. Valachovic, S. Ionov, Y. Wen, J. Segal, and C. Wittig, J. Chem. Soc., Faraday Trans. **89**, 1419 (1993).

[28] N. F. Scherer, L. R. Khundkar, R. B. Bernstein, and A. H. Zewail, J. Chem. Phys. **87**, 1451 (1987).

[29] I. R. Sims, M. Gruebele, E. D. Potter, and A. H. Zewail, J. Chem. Phys. **97**, 4127 (1992).

[30] R. D. van Zee, J. C. Stephenson, and M. P. Cassasa, Chem. Phys. Lett. **223**, 167 (1994).

[31] S.-I. Wada and K. Obi, J. Phys. Chem. **102**, 3481 (1997).

[32] S. I. Ionov, G. A. Brucker, C. Jacques, L. Valachovic, and C. Wittig, J. Chem. Phys. **99**, 6553 (1993).

[33] K. Kühl and R. Schincke, Chem. Phys. Lett. **158**, 81 (1989).

[34] R. Bersohn and M. Shapiro, J. Chem. Phys. **85**, 1396 (1986).

[35] Z. T. Cai, D. H. Zhang, and J. Z. H. Zhang, J. Chem. Phys. **100**, 5631 (1994).

[36] R. Bersohn and A. H. Zewail, Ber. Bunsenges. Phys. Chem. **92**, 373 (1988).

[37] G. H. Dieke and H. M. Crosswhite, J. Quant. Spectrosc. Radiat. Transf. **2**, 97 (1962).

[38] J. Brzozowski, P. Erman, and M. Lyyra, Phys. Scr. **17**, 507 (1987).

[39] I. L. Chidsey and D. R. Crosley, J. Quant. Spectrosc. Radiat. Transf. **23**, 187 (1980).

[40] R. N. Zare, *Angular Momentum* (Wiley, New York, 1988), p. 297 ff.

[41] J. T. Hougen, *The Calculation of Rotational Energy Levels and Rotational Line Intensities in Diatomic Molecules, NBS Monograph 115* (USGPO, Washington, DC, 1970).

[42] Y. Inagaki, Y. Matsumi, and M. Kawasaki, Bull. Chem. Soc. Jpn. **66**, 3166 (1993).

[43] C. L. Lin, N. K. Rohatgi, and W. B. DeMore, Geophys. Res. Lett. **5**, 113 (1978).

[44] A. Schiffman, D. D. Nelson, and D. J. Nesbitt, J. Chem. Phys. **98**, 6935 (1993).

[45] M. P. Docker, A. Hodgson, and J. P. Simons, Faraday Discuss. Chem. Soc. **82**, 1 (1986).

[46] R. N. Dixon, J. Nightingale, C. M. Western, and X. Yang, Chem. Phys. Lett. **151**, 328 (1988).

[47] M. P. Docker, A. Hodgson, and J. P. Simons, Chem. Phys. Lett. **128**, 264 (1986).

[48] K.-H. Gericke, A. U. Grunewald, S. Klee, and F. J. Comes, J. Chem. Phys. **88**, 6255 (1988).

[49] S. Klee, K.-H. Gericke, and F. J. Comes, J. Chem. Phys. **85**, 40 (1986).

[50] K.-H. Gericke, S. Klee, F. J. Comes, and R. N. Dixon, J. Chem. Phys. **85**, 4463 (1986).

[51] D. E. Freeman, K. Yoshino, J. R. Esmund, and W. H. Parkinson, Planet. Space Sci. **32**, 239 (1984).

[52] M. P. Casassa, J. C. Stephenson, and D. S. King, J. Chem. Phys. **89**, 1966 (1988).

[53] R. B. Bernstein and R. D. Levine, Adv. At. Mol. Phys. **11**, 215 (1975).

[54] W. Forst, Chem. Rev. **71**, 354 (1971).

[55] V. Spirko and P. R. Bunker, J. Mol. Spectrosc. **95**, 381 (1982).

[56] T. Baer and W. L. Hase, *Unimolecular Reaction Dynamics* (Oxford University Press, New York, 1996), p. 324 ff.

[57] J. L. Kinsey, J. Chem. Phys. **54**, 1206 (1971).

[58] See T. Baer and W. L. Hase, Ref. 56, p. 328 ff.

[59] See T. Baer and W. L. Hase, Ref. 56, p. 188 ff.

[60] The program ''A General RRKM Program,'' by W. L. Hase and D. L. Bunker, QCPE No. 234, was used to calculate RRKM rates for dissociation of CH_3OH. Transition state frequencies of 3682, 2947(2), 2846, 1479, 1455, 1427, 400, 300, 280 cm^{-1}, and TRM=TRC=7.5×10^{-3} amu nm^2 were used. These parameters fit the 5.4 ps appearance time-constant for the cluster experiment and the experimental high pressure Arrhenius A-factor, $A_\infty=1\times10^{16}$ s^{-1}.

[61] W. Tsang, Int. J. Chem. Kinet. **8**, 193 (1976).

[62] J. A. Blazy, D. A. King, and J. C. Stephenson (unpublished).

[63] M. Olzmann, Ber. Bunsenges. Phys. Chem. **101**, 533 (1997).

[64] O. V. Boyarkin, T. R. Rizzo, and D. S. Perry, J. Chem. Phys. **110**, 11346 (1999).

[65] R. I. Greenberg and J. Heicklen, Int. J. Chem. Kinet. **4**, 417 (1972).

[66] P. Michaud and R. J. Cvetanovic, J. Phys. Chem. **76**, 1375 (1972) and references therein.

[67] R. K. Sparks, L. R. Carlson, K. Shobatake, M. L. Kowalczyk, and Y. T. Lee, J. Chem. Phys. **72**, 1401 (1980). The $O(^1D_2)$ has a narrow speed distribution with about 90% of the atoms having speeds between $1.8-2.3\times10^5$ cm s^{-1}. The 1600 cm^{-1} of translational energy is such a small fraction of the available energy that the slight spread in speed should have an insignificant affect on the energetics and the formation times.

[68] J. Glownia, J. Misewich, R. Walkup, M. Kaschke, and P. Sorokin, Top. Appl. Phys. **70**, 3 (1992).

[69] A. H. Zewail, J. Phys. Chem. **100**, 12701 (1996).

[70] A. H. Zewail, Science **242**, 1645 (1988).

[71] E. A. Wade, H. Clauberg, S. K. Kim, A. Mellinger, and C. B. Moore, J. Phys. Chem. A **101**, 732 (1997).

[72] E. A. Wade, A. Mellinger, M. A. Hall, and C. B. Moore, J. Phys. Chem. A **101**, 6568 (1997).

[73] A. R. Hight Walker, G. T. Fraser, R. D. Suenram, and F. J. Lovas, J. Chem. Phys. **113**, 2139 (2000).

[74] C. Leforestier, F. LeQuere, K. Yamashita, and K. Morokuma, J. Chem. Phys. **101**, 3806 (1994).

[75] N. Balakrishnan and G. D. Billing, J. Chem. Phys. **101**, 2968 (1994).

[76] D. Chasman, D. J. Tannor, and D. G. Imre, J. Chem. Phys. **89**, 6667 (1988).

[77] A. G. Suits, R. L. Miller, L. S. Bontuyan, and P. L. Houston, J. Chem. Soc., Faraday Trans. **89**, 1443 (1993).

[78] J. J. Knudtson and J. C. Stephenson, Chem. Phys. Lett. **107**, 385 (1984), and works cited therein.

[79] C. Lugez, A. Schriver, R. Levant, and L. Schriver-Mazzuoli, Chem. Phys. **181**, 129 (1994).

[80] P. M. Aker, J. J. A. O'Brien, and J. J. Sloan, J. Chem. Phys. **84**, 745 (1986).

[81] S. G. Cheskis, A. A. Iogansen, P. V. Kulakov, I. Yu. Razuvaev, O. M. Sarkisov, and A. A. Titov, Chem. Phys. Lett. **155**, 37 (1989).

[82] Y. Hurwitz, Y. Rudich, and R. Naaman, Chem. Phys. Lett. **215**, 674 (1993).

[83] Y. Rudich, Y. Hurwitz, G. J. Frost, V. Vaida, and R. Naaman, J. Chem. Phys. **99**, 4500 (1993).

[84] G. M. Sweeney, A. Watson, and K. G. McKendrick, J. Chem. Phys. **106**, 9172 (1997).

[85] J. McFarlane, J. C. Polanyi, and J. G. Shapter, J. Photochem. Photobiol., A **58**, 139 (1991).

[86] G. M. Sweeney and K. G. McKendrick, J. Chem. Phys. **106**, 9182 (1997).

[87] S. P. Walsh and T. H. Dunning, Jr., J. Chem. Phys. **72**, 3221 (1980).

[88] D. C. Clary, Phys. Chem. Chem. Phys. **1**, 1173 (1999).

[89] J. C. Corchado, J. E.-Garcia, O. R.-Neto, Y.-Y. Chuang, and D. G. Truhlar, J. Phys. Chem. **102**, 4899 (1998).

[90] M. González, J. Hernando, J. Millán, and R. Sayós, J. Chem. Phys. **110**, 7326 (1999).

[91] P. Casavecchia, R. J. Buss, S. J. Sibener, and Y. T. Lee, J. Chem. Phys. **73**, 6351 (1980).

[92] I.-C. Chen, W. H. Green, Jr., and C. Bradley Moore, J. Chem. Phys. **89**, 314 (1988).

[93] P. R. Bunker, P. Jensen, W. P. Kraemer, and R. Beardsworth, J. Chem. Phys. **85**, 3724 (1986).

[94] S. Dóbé, T. Bérces, F. Temps, H. Gg. Wagner, and H. Ziemer, J. Phys. Chem. **98**, 9792 (1994).

[95] C.-F. Pau and W. J. Hehre, J. Phys. Chem. **86**, 1252 (1982).

[96] R. D. Johnson III and J. W. Hudgens, J. Phys. Chem. **100**, 19874 (1996).